

Asymptotically Normal Estimation of Local Latent Network Curvature

Steven Wilkins-Reeves ^{*1} and Tyler McCormick ^{†1,2}

¹Department of Statistics, University of Washington

²Department of Sociology, University of Washington

June 9, 2023

Abstract

Network data, commonly used throughout the physical, social, and biological sciences, consists of nodes (individuals) and the edges (interactions) between them. One way to represent network data’s complex, high-dimensional structure is to embed the graph into a low-dimensional geometric space. The curvature of this space, in particular, provides insights about the structure in the graph, such as the propensity to form triangles or present tree-like structures. We derive an estimating function for curvature based on triangle side lengths and the length of the midpoint of a side to the opposing corner. We construct an estimator where the only input is a distance matrix and also establish asymptotic normality. We next introduce a novel latent distance matrix estimator for networks and an efficient algorithm to compute the estimate via solving iterative quadratic programs. We apply this method to the Los Alamos National Laboratory Unified Network and Host dataset and show how curvature estimates can be used to detect a red-team attack faster than naive methods, as well as discover non-constant latent curvature in co-authorship networks in physics. The code for this paper is available at <https://github.com/SteveJWR/netcurve>, and the methods are implemented in the R package <https://github.com/SteveJWR/lolaR>.

1 Introduction

Social networks consist of a set of actors and the connections between them. Formally, a set of nodes (or vertices) $V = \{1, 2, \dots, n\}$ and edges $E \subset \{(i, j) | i \neq j, i \in$

*stevewr@uw.edu

†tylermc@uw.edu

$V, j \in V\}$ define a graph or network $G = (V, E)$. Beyond just the social network setting where these actors may represent individuals (e.g. Borgatti et al. [2009]), network models are used in many areas of the biological and physical sciences where the nodes may represent objects of interest such as cells (e.g. Bassett et al. [2018]), and particles (e.g. Papadopoulos et al. [2018]) respectively.

The high-dimensional, complex structure is an inherent feature of network data. This structure creates challenges in representing and modeling these rich data. One common approach uses embedding into lower-dimensional geometric spaces, where both properties of the geometric space and the position of points in the space reveal insights about the structure in the graph.

In this paper, we focus on the properties of the geometric space, particularly the notion of curvature. The sectional curvature of a latent space is, broadly defined, the deviation from a flat (Euclidean) space via the growth of the circumference of small circles as a function of their radius. Numerous previous approaches in this area have adopted a “discrete” approach, where the discreteness arises from the structure of the distance matrix between nodes (using path length). These curvature definitions include Ollivier-Ricci Curvature [Ollivier, 2007], Haantjes-Ricci curvature [Saucan et al., 2020] and Forman-Ricci curvature [Leal et al., 2018].

Despite some of their unknown statistical properties, these ideas have been useful in a variety of applications such as understanding financial network instability [Sandhu et al., 2016, Samal et al., 2021], network sampling [Barkanass et al., 2022], cancer detection in gene regulatory networks [Sandhu et al., 2015], functional neuroscience [Farooq et al., 2019] and community detection [Sia et al., 2019, Ni et al., 2019]. These definitions are motivated for networks defined as a static object and do not necessarily measure the curvature of the underlying latent space. Therefore it is not apparent what these estimates will converge to (or if they converge at all) when a network is studied as a random object.

Our approach deviates from these previous approaches to measuring curvature by developing a method that is explicitly linked to a particular model for network formation, the latent distance model of Hoff et al. [2002]. Defining curvature based on a specific probabilistic model yields a direct connection between curvature and the underlying properties of a generative model for the graph. Specifically, we develop a consistent and asymptotically normal estimator of the local curvature of the latent distance model, though our results for curvature estimation apply broadly to settings where distance matrices can be estimated. We also demonstrate that this estimator provides valuable insights when used in several existing statistical problems for network data. Specifically, we develop a hypothesis testing framework to reveal areas of non-constant curvature, which correspond to notions of brokerage in the sociology literature [Burt, 1992, Buskens and Van de Rijt, 2008]. We also demonstrate that our estimator can be used in changepoint detection with an application to cybersecurity.

Moving now to discuss the probabilistic framework in more detail, the latent distance model consists of locations Z_i, Z_j , most generally on some metric space, \mathfrak{M} , often taken to be a smooth Riemannian manifold \mathcal{M}^p where the probability of forming an edge $(i, j) \in E$ is inversely proportional to the distance on the latent manifold, $d_{\mathcal{M}}(Z_i, Z_j)$,

$$\tilde{g}\left(P\left((i, j) \in E\right)\right) \propto -d_{\mathcal{M}}(Z_i, Z_j)$$

where $\tilde{g}(\cdot)$ is some link function. The latent distance models and their extensions have been for such problems as modeling social influence [Sweet and Adhikari, 2020], social media relationships of politicians [Lok et al., 2021] and neuron connectivity [Aliverti and Durante, 2019] among numerous others. Where convenient, we condense $d_{\mathcal{M}}(x, y)$ with $d(x, y)$ or d_{xy} for brevity of notation.

The true latent geometry has implications for the global network properties. For example, spherical (positively curved) spaces form triangles and clusters more often than flat spaces, and hyperbolic (negatively curved) spaces tend to generate tree-like structures [Smith et al., 2017]. In other generative models of networks, the degree distribution and clustering of the network have implications of epidemic severity in network-based SIR models [Volz et al., 2011], suggesting links to other properties of interest among network data.

Lubold et al. [2023] constructed a method of identifying the latent curvature. However, this method requires first picking a sign of the curvature prior to estimation, relies on constant curvature globally, and does not admit a known asymptotic result. One study of discrete graph curvature from the physics literature illustrates consistency to a global manifold in a particular data-generating case [van der Hoorn et al., 2020]. The authors study the convergence of a modified Ollivier-Ricci curvature to the Ricci curvature of the underlying space in random geometric graphs under the limit of the connection radius shrinking to 0. Smith et al. [2017] also provide a method for identifying curvature based on simulations that compare the eigenspectrum of the graph Laplacian to models under spherical, hyperbolic, and Euclidean geometry.

The remainder of the paper continues as follows. First, in Section 2, we introduce the statistical model and manifolds of constant curvature. We then introduce the midpoint curvature equation, which allows for the identification of curvature given a set of distances. We follow up with some asymptotic theory when distances are estimated and an exact midpoint is present. We then establish convergence rates for midpoint set formation. In Section 4, we consider the practical estimation methods and illustrate consistency of our estimator.

Next, we discuss downstream statistical tasks such as a testing constant curvature in Section 5 and detecting changepoints in Section 6. We further elaborate on these with applications of these methods to co-authorship networks in physics and an application in cybersecurity.

2 Methods

We will begin with an introduction of the models under consideration, then follow up with an introduction of the estimator and the associated asymptotic theory. We follow this up with a discussion of the bias associated with a point that is not precisely the midpoint of two other points and discuss the rate of convergence of the best approximation to a midpoint of two other points. Lastly, we discuss the estimation of distance matrices in the generative network model.

2.1 Generative Model

We consider the random symmetric network corresponding to a graph $G = (V, E)$ where $|V| = n$, with adjacency matrix $A \in \{0, 1\}^{n \times n}$ such that $A_{ij} = 1$ iff $(i, j) \in E$. This random adjacency matrix is generated under a latent distance model [Hoff et al., 2002] with random effects (gregariousness parameters)

$$P(A_{ij} = 1 | \nu, Z) = \exp\left(\nu_i + \nu_j - d_{\mathcal{M}}(Z_i, Z_j)\right) \quad (1)$$

where

$$\begin{aligned} Z_i &\sim_{iid} F_Z \\ \nu_i &\sim_{iid} F_\nu \end{aligned}$$

with random effect measure (F_ν) with support on the non-positive real line $\text{supp}(F_\nu) \subset (\infty, 0]$ and where *iid* refers to sampling identically and independently from the latent distribution. This model relates the latent distances of the generative model to the probability of a connection between two points. Though not discussed in this paper, simple generalizations can be derived for directed networks. The latent position measure (F_Z) has support on some unknown latent manifold \mathcal{M}^p (of dimension p). This paper aims to estimate the curvature of \mathcal{M}^p . The $\exp(\cdot)$ link function is used as an example for ease of explanation, however in the supplementary materials we discuss the extension to the $\text{expit}(\cdot)$ model as well as possible further extensions.

Latent distance models *typically* assume a class of simply connected Riemannian manifolds of constant sectional curvature (κ), classically, the Euclidean \mathbb{E}^p , ($\kappa = 0$) and spherical $\mathbb{S}^p(\kappa)$, ($\kappa > 0$) and more recently the hyperbolic space $\mathbb{H}^p(\kappa)$ ($\kappa < 0$). However there are some extensions which are not restricted to this structure [Fosdick et al., 2016, Lok et al., 2021]. By the Killing-Hopf theorem [Killing, 1891], these are the only manifolds of constant sectional curvature. We will refer to these latent spaces as the **canonical manifolds**. These are selected for two reasons. Firstly there are techniques for visualization for each of these methods (for $p = 2$), thus highlighting the roles of individuals in the estimated model, and secondly, closed form expressions are available for the distances, allowing for estimation of these models. Embedding latent positions in a general Riemannian manifold would require the solving numerous variational optimization problems (computing geodesics/distances), preventing their use in practice. For a broader introduction on Riemannian geometry see Klingenberg [1995].

2.2 Models of Canonical Manifolds

Each of these canonical manifolds can be represented using a set of positions with real-valued vectors and a corresponding distance function. We include definitions for Euclidean, spherical, and hyperbolic spaces for completeness.

The Euclidean manifold will be equipped with the standard ℓ_2 norm \mathbb{E}^p which describes the set of points for which $x, y \in \mathbb{R}^p$ with distance matrix

$$d_{\mathbb{E}^p}(x, y) = \sqrt{\sum_{k=1}^p (x_k - y_k)^2}$$

The spherical model with curvature $\kappa > 0$ is equivalent to the sphere of radius $r = \frac{1}{\kappa^2}$. A simple way of expressing this is via the following model. A set of points are embedded in \mathbb{S}^p if $x \in \mathbb{R}^{p+1}$, $\sum_{k=0}^p x_i^2 = 1$. We add a zero indexed coordinate for the spherical and hyperbolic models. We compute a signature $B_{\mathbb{S}^p}$ and distances are computed via the signature

$$B_{\mathbb{S}^p}(x, y) = \sum_{k=0}^p x_i y_i$$

$$d_{\mathbb{S}^p}(x, y) = \frac{1}{\sqrt{\kappa}} \operatorname{acos}(B_{\mathbb{S}^p}(x, y))$$

The hyperboloid model with curvature $\kappa < 0$ corresponds to a set of points in \mathbb{H}^p if $x \in \mathbb{R}^{p+1}$, $x_0^2 - \sum_{k=1}^p x_i^2 = 1, x_0 > 0$. An analogous signature $B_{\mathbb{H}^p}$ exists for the hyperbolic embedding.

$$B_{\mathbb{H}^p}(x, y) = x_0 y_0 - \sum_{k=1}^p x_i y_i$$

$$d_{\mathbb{H}^p}(x, y) = \frac{1}{\sqrt{-\kappa}} \operatorname{acosh}(B_{\mathbb{H}^p}(x, y))$$

In our setting, we do not require \mathcal{M}^p to have constant curvature, but we do make some much more mild assumptions on \mathcal{M}^p . We consider $\mathfrak{M} = (\mathcal{M}^p, d)$ the metric space induced by the Riemannian manifold.

- (A1) (**Algebraic Midpoint Property**) \mathfrak{M} satisfies the algebraic midpoint property. For any $x, y \in \mathcal{M}^p$ there exists a point z such that $d_{\mathcal{M}^p}(z, x) = d_{\mathcal{M}^p}(z, y) = \frac{1}{2} d_{\mathcal{M}^p}(y, x)$.
- (A2) (**Locally Euclidean**) For all $p \in \mathcal{M}^p$ there exists some $\delta > 0$ and some c_p, C_p such that for all $\epsilon \leq \delta$:

$$c_p(\delta) \leq \frac{\operatorname{Vol}(B_{\mathcal{M}^p}(\epsilon, q))}{\operatorname{Vol}(B_{\mathbb{E}^p}(\epsilon, 0))} \leq C_p(\delta)$$

and

$$\lim_{\epsilon \rightarrow 0} \frac{\operatorname{Vol}(B_{\mathcal{M}^p}(\epsilon, q))}{\operatorname{Vol}(B_{\mathbb{E}^p}(\epsilon, 0))} = 1$$

where $B_{\mathcal{M}^p}(\epsilon, q)$ is the ϵ ball on \mathcal{M}^p centred at a point q . Unless otherwise specified, from here if denoting $B(\epsilon, q)$ we are referring to the ball on the latent manifold \mathcal{M}^p .

If \mathcal{M}^p is a connected manifold with sectional curvature upper and lower bounded, then these properties are satisfied. See Section E in the supplementary materials for details.

2.3 Curvature and Estimating Equation

A number of methods exist to verify whether a particular set of distances can be embedded in a space of constant curvature. These include Schoenberg [1935] and Begelfor and Werman [2005] as well as Cayley-Menger determinants [Blumenthal and Gillam, 1943]. Lubold et al. [2023] previously used these methods in order identify whether a set of distances could be globally embedded in a particular curvature

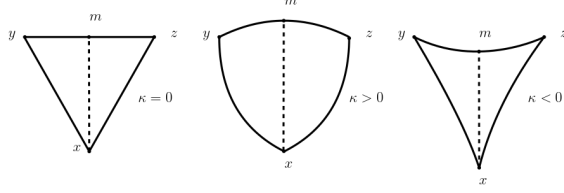


Figure 1: Midpoint distances and curvature of the space. The distance d_{xm} is an increasing function of the curvature κ for fixed other triangle side lengths.

space. In this work, we take a different approach where we can identify curvature based on a minimal set of points.

We rely on a simple geometric insight. Consider a set of three points that form a triangle. If we look at the midpoint of any of the sides of this triangle, we can construct a distance from the midpoint to the opposite vertex. This length reveals the sectional curvature of the manifold, where a smaller distance corresponds to a more negatively curved space and a larger distance corresponding to a more positively curved space. This is visualized in Figure 1 for Euclidean, spherical and hyperbolic triangles.

This use of midpoints will help us identify the curvature of the latent space. For example, consider a case where no midpoint is present in the data. We let 4 points placed equidistant from each other, we can either embed these in \mathbb{E}^3 or $\mathbb{S}^2(\kappa)$ for $\kappa > 0$. Therefore the curvature of the latent space cannot be identified from this configuration. Though conditions like Schoenberg’s, [Schoenberg, 1935] which are used in Lubold et al. [2023] can determine whether a distance matrix can be embedded in a space of constant curvature, identifiability concerns remain.

We instead take a much more direct approach at eliciting curvature, through the use of the existence of a midpoint. This lets us identify a curvature with only 4 points in total. The use of a midpoint allows us to work with a sub-manifold of dimension 2 which as long as $p \geq 2$ will allow for identification of the curvature, circumventing the need to identify the dimensionality of the latent space. We will introduce an estimator for the curvature of the latent space and derive its asymptotic distribution in the case of a known midpoint. We follow this up with a discussion regarding the convergence rate of surrogate (approximate) midpoints.

We now formalize this intuition. For any 3 points x, y, z which lie in an unknown Riemannian manifold of dimension $p \geq 2$ of constant sectional curvature κ , (x, y, z) can be isometrically embedded in a sub-manifold of dimension 2.

Definition 1. *A submanifold $\tilde{\mathcal{M}} \subset \mathcal{M}$ is totally geodesic if every geodesic in $\tilde{\mathcal{M}}$ is also a geodesic in \mathcal{M} .*

We will use the fact that a totally geodesic submanifold contains all points along the geodesic, including the midpoint.

Lemma 1. *For any $x, y, z \in \mathcal{M}^p(\kappa)$ if m is a midpoint lying between y and z . Then $x, y, z, m \in \mathcal{M}^2(\kappa)$ where $\mathcal{M}^2(\kappa)$ is a totally geodesic submanifold of dimension 2.*

The proof is straightforward and in Section A.1. The main implication here is that the totally geodesic submanifold allows us to look at distances in a subspace

of dimension 2 which allow for identification. The three points x, y, z will fall into one of these sub-manifolds, m which lies on the geodesic between y and z . Since geodesics determine the distance, and geodesics on the submanifold are the same as geodesics on the total manifold, then this gives a criteria for identifying the latent curvature through the fortunate alignment of midpoints.

We now use this fact to derive an equation which will relate the curvature κ to the set of distances between the points (x, y, z, m) .

Theorem 2 (Midpoint Curvature Equation). *Suppose that points $x, y, z \in \mathcal{M}^p(\kappa)$ an unknown Riemannian manifold of dimension p of constant sectional curvature κ . Let m denote the midpoint between y, z . The following equation holds for $\kappa \in \mathbb{R}$.*

$$g(\kappa, d) = \operatorname{Re} \left[\frac{2 \cos(d_{xm} \sqrt{\kappa})}{\kappa} - \frac{\sec(\frac{d_{yz}}{2} \sqrt{\kappa}) (\cos(d_{xy} \sqrt{\kappa}) + \cos(d_{xz} \sqrt{\kappa}))}{\kappa} \right] = 0 \quad (2)$$

Where d_{jk} denoted the distance between points j, k and $\operatorname{Re}[\]$ denotes the real part of the equation.

For cases when $\kappa < 0$, we take the real part of the above equation, which is equivalent to replacing the trigonometric functions with their hyperbolic analogues. Naturally, this can also be solved for d_{xm} to compute the distance to the midpoint in a space of constant curvature $d_{xm}(\kappa'; \mathbf{d}(x, y, z))$.

The proof is found in the supplementary materials in Section A.2. In essence, this equation is related to Toponogov's theorem (Klingenberg [1995] 2.7.12), which can be used to define a parameter based on distances θ_T based on distances of a triangle x, y, z .

$$\theta_T(d) := \frac{1}{2}d_{xz}^2 + \frac{1}{2}d_{xy}^2 + \frac{1}{4}d_{yz}^2 - d_{xm}^2.$$

If the sectional curvature of \mathcal{M}^p is non-negative, then $\theta_T(d) \geq 0$ and if the curvature is non-positive $\theta_T(d) \leq 0$. In Euclidean space, this reduces to the parallelogram law. Toponogov's theorem itself does not identify curvature, but if we assume that the points $x, y, z, m \in \mathcal{M}^2(\kappa) \subseteq \mathcal{M}^p$ a totally geodesic submanifold of dimension 2 which is simply connected and of constant curvature, then this set of distances can be used to identify the curvature. The important distinction between this method of identification via Schoenberg [1935] or through Cayley-Menger determinants [Blumenthal and Gillam, 1943] is that these do not include the information of a midpoint whereas ours does. Additionally, these embedding theorems do not necessarily allow for the unique identification of curvature, but rather if a particular space of constant curvature can embed a given distance matrix.

To highlight the smoothness of our estimating function we plot a set of examples. For a unit equilateral triangle, we compute the corresponding midpoint distance d_{xm} for each curvature space with $\kappa \in \{-2, -1, 0, 1, 2\}$. We see in Figure 2 that our proposed estimating equation is differentiable around the solution with non-zero derivative, allowing one to identify the curvature from the $\kappa : g(\kappa, d) = 0$.

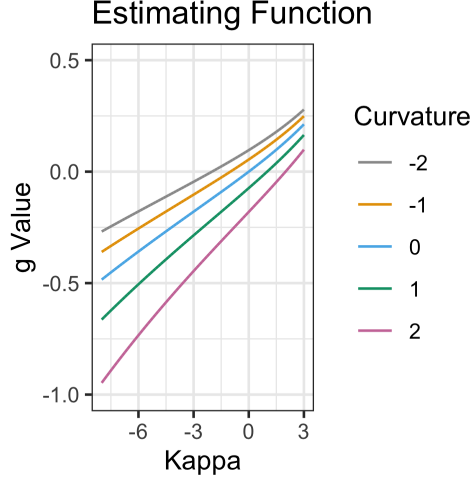


Figure 2: Example of estimating functions g as a function of κ .

2.4 Curvature Estimation

Now that we have an estimating function which allows us to identify curvature, we discuss the estimator's asymptotics.

Theorem 3. *Suppose there exist points $x, y, z \in \mathcal{M}^p$. Let m denote the midpoint between y, z where these points are fixed. Let $\hat{\mathbf{d}} = (\hat{d}_{xy}, \hat{d}_{xz}, \hat{d}_{yz}, \hat{d}_{xm})$ be the estimated distances and $\mathbf{d} = (d_{xy}, d_{xz}, d_{yz}, d_{xm})$ be their true, unknown counterparts. Assume we have a distance estimator such $\hat{\mathbf{d}}$ and*

- (B1) $\sqrt{r(n)}(\hat{\mathbf{d}} - \mathbf{d}) \rightarrow N(0, \Sigma)$
- (B2) $\kappa < \left(\frac{\pi}{\max\{d_{xy}, d_{xz}, d_{yz}, d_{xm}\}} \right)^2$
- (B3) $\left. \frac{d}{d\kappa'} d_{xm}(\kappa'; \mathbf{d}(x, y, z)) \right|_{\kappa'=\kappa} > 0$

Where $r(n)$ is the rate of convergence. Let $\hat{\kappa}$ to the solution to of $g(\kappa, \hat{\mathbf{d}}) = 0$. Then

$$\sqrt{r(n)}(\hat{\kappa} - \kappa) \rightarrow_d N \left(0, \left(\frac{\partial g(\kappa, \mathbf{d})}{\partial \kappa} \right)^{-2} \left(\nabla_d g(\kappa, \mathbf{d})^\top \Sigma \nabla_d g(\kappa, \mathbf{d}) \right) \right) \quad (3)$$

where \rightarrow_d refers to convergence in distribution. If (B1) is replaced by consistency, i.e. $\|\hat{\mathbf{d}} - \mathbf{d}\|_2 = o_P(r(n)^{-1/2})$, then $\hat{\kappa} - \kappa = o_P(r(n)^{-1/2})$.

The proof is found in the supplementary materials in Section A.3 and is an application of the implicit function theorem and the delta method. Assumption (B1) is mild as it only requires asymptotic normality of the distance estimator. Assumption (B2) is mild as it requires all of the distances to be embeddable on the sphere of curvature κ . Assumption (B3) tends to hold unless the three points x, y, z are co-linear. For a more in depth discussion of the non-decreasing property of the midpoint, see Lemma 12 in the appendix. In our applications we will find that $r(n) = \ell^2$, where ℓ is the size of the cliques used to construct the distance matrix. However if one has

distance estimates at a faster rate, then these can be plugged in to obtain faster curvature estimates. Moreover, this is general to many problems where distances are being estimated. Of course, this requires the knowledge of a true midpoint as well. In the following sections, we discuss the use of approximate midpoints, as well as introduce techniques for estimating distances on the underlying manifold of model (equation (1)).

2.5 Midpoint Bias

Until this point we have worked under the assumption that there is a known midpoint for a particular pair of points. However, in general, this is not known. Suppose that m' is a point which is a *surrogate midpoint* (m') for the midpoint between y, z and we have the analogous distance $d_{xm'}$. By a Taylor series expansion:

$$\begin{aligned} 0 &= g(\kappa', d') - g(\kappa, d) \\ &= \nabla_{\kappa} g(\kappa, d)(\kappa - \kappa') + \nabla_{d_{xm}} g(\kappa, d)(d_{xm} - d_{xm'}) \\ &\quad + o(|\kappa - \kappa'|) + o(|d_{xm} - d_{xm'}|) \\ \implies |\kappa - \kappa'| &\approx (\nabla_{\kappa} g(\kappa, d))^{-1} \nabla_{d_{xm}} g(\kappa, d) |d_{xm} - d_{xm'}| \\ &\leq (\nabla_{\kappa} g(\kappa, d))^{-1} \nabla_{d_{xm}} g(\kappa, d) d_{mm'} \end{aligned}$$

Hence, the bias will scale approximately linearly as a function of $d_{mm'}$ for small values of $d_{mm'}$.

We next provide an outline involving how fast we can expect surrogate midpoints form. We first introduce the definition of geodesic convexity. A subset $A \subset \mathcal{M}^p$ is geodesically convex if the geodesic between any two points in A , is contained within A itself. Here convexity on a manifold will refer to geodesic convexity. In the following theorem, let $f_{m,3}(m_1, m_2)$ denote the joint density function of a pair of midpoints with a shared endpoint, and let $f_{m,4}(m_1, m_2)$ denote the joint density of two midpoints without an endpoint shared. These two densities will be functions of the unknown manifold, \mathcal{M} and the distribution on the latent positions Z .

Theorem 4. *Suppose that $Z_i \stackrel{iid}{\sim} F_Z$ are K points sampled iid from an unknown latent distribution on a simply connected manifold \mathcal{M}^p . Denote this set of points $\{Z_i\}_{i=1}^K = \mathcal{D}_K$ Suppose there exists a convex region A for which*

- (C1) $f(z) \geq \alpha > 0$, for all $z \in A$
- (C2) $\dim(A) = p \geq 2$
- (C3) $f_{m,3}(m_1, m_2), f_{m,4}(m_1, m_2) \leq \alpha_m < \infty$

for all $z \in A$ where f is the density function corresponding to F_Z .

Define the statistic

$$\Phi(\mathcal{D}_K) := \min_{x,y,z \in \mathcal{D}: x \neq y, x \neq z, y \neq z} d(m(y, z), x)$$

Then

$$\Phi(\mathcal{D}_K) = \mathcal{O}_P(K^{-3/p}) \tag{4}$$

Our approach to showing the above result draws on similarities to Cai et al. [2013] and Brauchart et al. [2015] which discuss convergence of the minimum distance between any two points sampled uniformly on a hypersphere. The authors show that $\min_{i,j} d(Z_i, Z_j) = \mathcal{O}_P(K^{-2/p})$, though they also derive an exact distribution for $\min_{i,j} d(Z_i, Z_j)$ using the extra assumption of uniformity on the sphere. The authors use a technique by recursively computing the probability that a point is at least a radius ϵ away from the previous K points. Since at each placement of a new point, there are $\binom{K}{2}$ midpoints as opposed to K current points, leading to the faster rate we observe.

Assumption (C1) ensures that there does exist a geodesically convex regions which midpoints can form. Assumption (C2) ensures that this region is equal to the dimension of the ambient space. Lastly, assumption (C3) is relatively mild so long as we have a smooth manifold and a continuous latent density. The proof is left to the Section A.6 in the supplementary materials but relies on the following Theorem regarding medians of arbitrarily correlated random variables which may be of independent interest.

Theorem 5. *Consider a set of continuous random variables $X_i \in \mathbb{R}$ which are marginally identical but have an arbitrary dependency. Let $\widehat{\mathbb{M}}[X]$ denote the sample median of the set of these random variables. Then*

$$P(\widehat{\mathbb{M}}[X] \leq t) \leq 2P(X \leq t) \quad (5)$$

We find the proof in the supplementary materials in Section A.5. This bound is only useful up to $t = \mathbb{M}[X]$ at which point the upper bound is 1. The implication here is that we only need most of the midpoints between any two points to be reasonably separated. We later illustrate how we will find good midpoints and so we can verify their existence in any observed dataset.

2.6 Upper and Lower Bounds on the Curvature

We have shown above that under some mild conditions, we will find good midpoints eventually. There are, however, some cases, such as some distributions F_Z defined on discrete domains on the latent manifold, for which good midpoints are not guaranteed to form. Additionally, under any finite sample, we will not have an exact midpoint alignment. To alleviate these issues we use a similar strategy to derive upper and lower bounds for the curvature as long as the surrogate midpoint exists in the same region of constant curvature.

Theorem 6 (Curvature Bounds). *Let $x, y, z, m' \in \mathcal{M}^p(\kappa)$ where m' need not be the exact midpoint of y and z , but rather a surrogate midpoint. Then let d_{jk} denote the distance between points $j, k \in \{x, y, z, m'\}$. Let κ_u and κ_l denote the solutions*

$$\begin{aligned} g(\kappa_u, \mathbf{d}(x, y, z), d_{xm'} + d_{mm'}(\kappa_u, \mathbf{d}(m', y, z))) &= 0 \\ g(\kappa_l, \mathbf{d}(x, y, z), d_{xm'} - d_{mm'}(\kappa_l, \mathbf{d}(m', y, z))) &= 0 \end{aligned}$$

then $\kappa_l \leq \kappa \leq \kappa_u$.

If $d_{mm'}(\kappa, \mathbf{d}(m', y, z)) = 0$ then the upper and lower bounds converge. Similar to the curvature estimate $\widehat{\kappa}$, given a noisy estimate of the distances, we can estimate the upper and lower bounds of the curvature. We will primarily use this for constant curvature testing as we will see in Section 5.

3 Distance Matrix Estimation

In the previous section, we have not required any distances related to the latent distance model, but rather arbitrary sets of distances. In this section we introduce a method for estimating a distance matrix under the latent distance model. If we knew the curvature of the manifold, we could use maximum likelihood or other statistical techniques to estimate latent positions and, therefore the latent distances. This approach is commonly used in practice when the manifold geometry is assumed *a priori*. In our case, however the goal is to estimate the underlying curvature, so we need a notion of distance that is consistent across geometries.

We exploit a similar strategy to Lubold et al. [2023] in constructing a distance matrix. Specifically, we construct distances using connections across cliques, or fully connected subgraphs. This approach has two advantages. First, since cliques represent multiple nodes we have multiple opportunities for there to be connections between two cliques, meaning we can use the fraction of realized ties between two cliques as an estimate for the probability of connection between the two cliques. Since our approach relies on a specific probability model for connections, we can easily convert connection probabilities into distances using the parametric model. Second, in general, cliques will correspond to points near each-other in space. This means that we can consider cliques as “points” on the manifold that can be used to identify a distance matrix.

We now proceed to describe our approach in detail. In order to estimate the distance matrix, we first assume we have access to the person-specific effects and focus only on the distances. We later relax this as it will be negligible if we can estimate them at a fast enough rate. Under this model, we nodes within a clique have nearly the same latent position. We will also for illustration purposes here, first assume that this holds, and later illustrate the rate at which the diameter of the set of latent positions within a clique converges. Let $X, Y \in \{1, 2, \dots, n\}$ denote sets of nodes which denote non-overlapping cliques. Then the average probability of connection can be used to identify the latent distance, if we can also estimate the average of random effects (ν). Let $|W|$ denote the size of $W \in \{X, Y\}$. We define the average probability of connection across cliques X, Y as the following.

$$\begin{aligned}
 p_{XY} &:= \frac{1}{|X||Y|} \sum_{x \in X} \sum_{y \in Y} p_{xy} \\
 &= \frac{1}{|X||Y|} \sum_{x \in X} \sum_{y \in Y} \exp(\nu_x + \nu_y - d_{xy}) \\
 &= \exp(-d_{xy}) \frac{1}{|X||Y|} \sum_{x \in X} \sum_{y \in Y} \exp(\nu_x + \nu_y) \\
 \implies d_{xy} &= -\log(p_{XY}) + \gamma_X + \gamma_Y \\
 \gamma_W &:= \log \left(\frac{1}{|W|} \sum_{w \in W} \exp(\nu_w) \right) \quad \text{for } W \in \{X, Y\}
 \end{aligned}$$

Since there are ℓ^2 possible connections between a pair of cliques of size ℓ , we can construct an asymptotically normal estimator of p_{XY} by just the plug in sample average of connections. However, in order for these asymptotics to hold, we must estimate γ_X and γ_Y at rates $o_P(\frac{1}{\ell})$, so that these are asymptotically negligible nuisance

parameters. A final issue that remains however is the restriction of all distance estimates to ensure that they preserve the properties of a metric. We will illustrate our solutions to these problems in the following sections.

Unless latent positions are nearly (or exactly) in the same location, large cliques are rare in latent space models. The next lemma illustrates a rate of convergence of these latent locations relative to the size of a clique.

Lemma 7. *Assume the latent distance model as in equation (1) $\delta = \max_{i,j} d(Z_i, Z_j)$ and let C_ℓ denote the event that nodes $i = 1, \dots, \ell$ form a clique.*

Let $\mu_d = \mathbb{E}[d(Z_i, Z_j)]$ where Z_i and Z_j are drawn independently from F_Z . Then for any $0 < \tilde{\mu}_d < \mu_d$, if

- (D1) F_Z admits a continuous density f_Z

$$\delta|C_\ell = o_P(\exp(-\tilde{\mu}_d\ell)).$$

See the supplementary materials Section A.8 for a proof. The main implication is that it is reasonable to treat the latent positions as a single point when nodes are within a clique. The assumption in Lemma 7 ensures that we have some region in the latent space where positions can be drawn near each other, if there is a point mass anywhere on the latent space, then this condition is immediately satisfied, otherwise, if F_Z admits a smooth continuous density (f_z) then it is also satisfied in any region of positive density value, since \mathcal{M}^p satisfies the locally Euclidean property (A2).

In order to estimate d_{xy} we must estimate the nuisance parameters γ_X and γ_Y at a fast enough rate. If a set of nodes are generated from a common point, as in a clique, we can use the number of connections a point has to the rest of the network in order to identify the relative difference in their random effects. We assume that all points within a clique share the same latent position. We show in Lemma 7 that this assumption is reasonable as the latent radius of the points shrinks exponentially fast. Consider a set of nodes $i \in X$ where X denotes the indices of a clique. Let k denote the indices of any other node in the network. Then we can identify the differences of random effect values within a clique

$$\begin{aligned} P(A_{ik} = 1) &= \int \exp(\nu_i + \nu_k + d(z_i, z_k)) dF_Z(z_k) dF_\nu(\nu_k) \\ &= \exp(\nu_i) \int \exp(\nu_k + d(z_i, z_k)) dF_Z(z_k) dF_\nu(\nu_k) \\ \implies \frac{P(A_{ik} = 1)}{P(A_{jk} = 1)} &= \exp(\nu_i - \nu_j). \end{aligned}$$

Other than in pathological cases, $\ell \ll n$ where n is number of nodes in the network. As a result, we are able to measure the differences between the random effects of members of a clique quite effectively, at a rate of $O_P(\frac{1}{\sqrt{n}})$. Therefore, we can define $\nu_i = \nu_X + \Delta\nu_i$ which allows us to identify $\Delta\nu_i$ if $\nu_X = \min_{i \in X} \nu_i$ were known,

$$\gamma_X = \nu_X + \log \left(\frac{1}{|X|} \sum_{i \in X} \exp(\Delta\nu_i) \right).$$

The remaining question is to estimate ν_X . We will argue that the smallest random effect under mild conditions will converge to 0 at an exponentially fast rate.

Lemma 8. *Let C_ℓ denote the event that $i \in \{1, 2, \dots, \ell\}$ form a clique. Suppose that*

1. (E1) F_ν admits a continuous density (f_ν) on $(-\infty, 0]$ and $f_\nu(0) > 0$

Let $\mu_\nu := E[\nu]$. Then for any $\mu_\nu < \tilde{\mu}_\nu < 0$

$$\min_i \nu_i | C_\ell = o_P(\exp(-|\tilde{\mu}_\nu|\ell)) \quad (6)$$

This theorem states that the nodes which we find in a clique, tend to have near 0 random effects, and thus it is reasonable to set $\max_i \nu_i = 0$, when estimating the random effects. Note that this is an exponential rate which can be arbitrarily close to $(\exp(-|\mu_\nu|\ell))$.

Lemma 9. *Let $W \subset \{1, 2, \dots, n\}$ denote a subset of indices which form a clique (C_ℓ). Let d_i denote the degree of node $i \in W$ where $|W| = \ell$ and assume that the points in the clique have a common latent position. Denote the estimator of γ_W . Let $\mu_\nu := E[\nu]$. Then for any $\mu_\nu < \tilde{\mu}_\nu < 0$*

$$\hat{\gamma}_W = \log \left(\frac{1}{\ell} \sum_{i \in W} \frac{d_i}{\max_{j \in W} d_j} \right).$$

Then if (E1) in Lemma 8 holds, then define $\tilde{\mu}_\nu$ as in Lemma 8

$$\hat{\gamma}_W - \gamma_W = \mathcal{O}_P \left(\max \left\{ \exp(\tilde{\mu}_\nu \ell), \frac{1}{\sqrt{n}} \right\} \right) \quad (7)$$

Therefore, estimation of γ_W within a clique can occur at an exponential rate, meaning that this estimation will be negligible compared to the average cross-clique probabilities.

Theorem 10. *Let \hat{d} be a set of clique distances measured via connections between cliques of size ℓ with fixed positions x and y respectively. Assume that we have indices of cliques X, Y for which $|X| = |Y| = \ell$ and $X \cap Y = \emptyset$. We also assume the nuisance estimators exist for γ_W (condition F1) and that the Lindeberg CLT condition is satisfied for the counts between cliques*

- (F1) $\hat{\gamma}_W - \gamma_W = o_P(\frac{1}{\ell})$ for $W \in X, Y$
- (F2) $\lim_{\ell \rightarrow \infty} \frac{\sum_{x \in X} \sum_{y \in Y} (A_{xy} - p_{xy})^2 I(|A_{xy} - p_{xy}| > \epsilon \ell^2 \sigma_\ell)}{\sigma_\ell} = 0$
for all $\epsilon > 0$

Where

$$p_{XY} = \frac{1}{\ell^2} \sum_{x \in X} \sum_{y \in Y} p_{xy} \quad (8)$$

$$\sigma_\ell = \frac{1}{\ell^2} \sum_{x \in X} \sum_{y \in Y} p_{xy} (1 - p_{xy}) \quad (9)$$

Then

$$\sqrt{\ell^2 \frac{\sigma_\ell}{p_{XY}}} \left(\hat{d}_{xy} - d_{xy} \right) \rightarrow_d N(0, 1) \quad (10)$$

The conditions (F1) simply states that we have estimators of the nuisance parameters, and (F2) simply states that we have the standard Lindeberg condition for the central limit theorem when random variables are independent, but not necessarily identical. The proof is found in Section A.4. The main implication here is that if we can estimate the random effects fast enough within a clique, then we are able to estimate the random effects at a rate which is negligibly fast compared to the rate of \hat{p}_{XY} . Additionally, we note that since in general, the random effects are all converging to 0 within a clique, that for large cliques $p_{XY} \approx \exp(-d_{XY})$, thus allowing for simplified expressions for σ_ℓ and p_{XY} .

For a set of cliques $\mathcal{C} : |\mathcal{C}| = K$, we can compute a distance matrix $\hat{D} \in \mathbb{R}^{K \times K}$ such that we best fit the observed data while maintaining the restriction of the triangle inequalities. In this characterization and also in Lubold et al. [2023], the distance matrix estimation does not in fact necessarily respect the restrictions that all distance matrices must satisfy, namely non-negativity, and the triangle inequality. For example, we construct an enumeration of the cliques of size 7 or greater from the General Relativity co-authorship network of Leskovec et al. [2007] in Figure 3. Any pair of cliques which does not share an edge will inherently be estimated to have infinite distance, which prevents estimation of curvature. However applying the triangle inequality via other estimated distances in the graph would allow us to construct an upper bound. This is a challenge observed in Lubold et al. [2023], which required cliques that are pairwise connected.

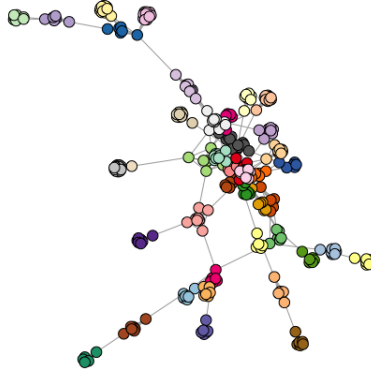


Figure 3: Clique subgraph of co-authorship network in ArXiv General Relativity. Cliques shown by color.

To address this challenge, we posit a similar estimation problem, while respecting the triangle inequality. The following estimation problem is posed below. Let X denote a set of indices corresponding to a single clique in a graph G . Let \mathcal{C} denote the set of cliques in an observed graph. Given a set of fixed effects, we can propose a maximum likelihood optimization problem for the distance matrix $D \in \mathbb{R}^{K \times K}$ under the generative model. By the approximation that cliques have a common latent

position, we define the following likelihood function of the clique subset of the data $\ell_{\mathcal{C}}$

$$\begin{aligned} \ell_{\mathcal{C}}(D; \boldsymbol{\nu}) &= \sum_{X, Y \in \mathcal{C}, i \in X, j \in Y} A_{ij} (\nu_i + \nu_j - d_{xy}) \\ &+ \sum_{X, Y \in \mathcal{C}, i \in X, j \in Y} (1 - A_{ij}) \log(1 - \exp(\nu_i + \nu_j - d_{xy})). \end{aligned}$$

Then we can define the maximum likelihood optimization problem, after estimating a set of random effects $\hat{\boldsymbol{\nu}}$

$$\begin{aligned} \hat{D} &= \sup_{D \in \mathbb{R}^{K \times K}} \ell_{\mathcal{C}}(D; \hat{\boldsymbol{\nu}}) \\ \text{s.t. } &d_{xy} \geq 0, \quad \text{Diag}(D) = 0, \quad \text{tr}(E_s^{\top} D) \geq 0 \forall s \in \mathcal{S} \end{aligned}$$

where \mathcal{C} is a list of clique indices and E_s are matrices full of zeros other than 3 indices, i, j, k for which $E[i, j] = E[i, k] = 1 = -E[j, k]$. This set of indices allows us to respect the triangle inequality for all possible triplets of distances. We define \mathcal{S} to be an enumeration of all such indices E_s . There are $3 \binom{K}{3}$ such restrictions. The set of feasible distance matrices that satisfy these constraints form a polyhedron of interior dimension $\binom{K}{2}$. This optimization procedure is a convex problem under the space of symmetric matrices with many restrictions. In practice, we use CVXR to solve this system [Fu et al., 2020]. For a greater gain in computational speed, we use the MOSEK solver for the constrained optimization [Andersen and Andersen, 2000].

Though in its current form, the problem is numerically challenging to solve due to the number of restrictions. A natural option is to approximate the likelihood via a second order Taylor expansion and solve this problem successively. This is exactly Newton's method. Since the Hessian is diagonal, $\frac{\partial^2}{\partial d_{ij} \partial d_{kl}} \ell_{\mathcal{C}}(D; \boldsymbol{\nu}) = 0$ if $d_{ij} \neq d_{kl}$, this can be made into a more efficient quadratic program which can be solved faster in CVXR.

Let $g(D; D_0; \boldsymbol{\nu})$ be the second order Taylor series approximation to $\ell_{\mathcal{C}}$ about a matrix D_0 . We can successively solve for \hat{D}_{t+1} the following constrained optimization problem

$$\begin{aligned} \hat{D}_{t+1} &= \sup_{D \in \mathbb{R}^{K \times K}} \tilde{g}(D, \hat{D}_t; \hat{\boldsymbol{\nu}}) \\ \text{s.t. } &d_{xy} \geq 0, \quad \text{Diag}(D) = 0, \quad \text{tr}(E_s^{\top} D) \geq 0 \forall s \in \mathcal{S} \end{aligned} \tag{11}$$

which can be iteratively computed until $\ell_{\mathcal{C}}$ increases less than some threshold. Each iteration is a linear constrained quadratic program which we implement in CVXR. For further details, see the supplementary materials in Section B.2.

3.1 One-Step Estimation

In practice, running the optimization step for many iterations can be computationally costly. This is particularly problematic in bootstrap testing for constant curvature (Section 5) It is well known in maximum likelihood estimation, one only needs to perform one Newton step for asymptotic efficiency [Le Cam, 1956]. As a result, one can start with any consistent estimator of the distance matrix D and apply a single Newton step from equation (11) and obtain the same asymptotic distribution, and therefore in practice, only one step is needed.

4 Practical Considerations and Statistical Tests

In this section we consider some of the practical issues with estimation. In particular, how to choose a good midpoint, and how to filter points which we know to have extremely high variance. In general, we would like to find a set of points for which $\widehat{d}_{ym} \approx \widehat{d}_{zm} \approx \frac{1}{2}\widehat{d}_{yz}$ with \widehat{d}_{yz} not excessively small.

4.1 Choosing Best Midpoint

In practice given a distance matrix we would like search over the space to find the best midpoint. For an unknown latent geometry, we can exploit the Fréchet mean of two points

$$m^* = \arg \min_{m \in \mathcal{M}} d_{ym}^2 + d_{zm}^2.$$

The midpoint between any two points y, z is also the Fréchet mean. Therefore we can search over the space of candidate entries of a distance matrix D to find the best midpoint available. In practice, we also would like to ensure that the points y, z are not too close to each-other. If y and z are too close to each-other, then this leads to a very high variance estimator. So a reasonable option is to normalize this quantity by d_{yz} . Given a true midpoint m^* , then $d_{ym^*} = d_{zm^*} = \frac{1}{2}d_{yz}$, then

$$\frac{d_{ym^*}^2 + d_{zm^*}^2}{d_{yz}^2} = 1/2 \quad (12)$$

Therefore in order to compute the best surrogate midpoint set we solve the following problem

$$\widehat{y}, \widehat{z}, \widehat{m} = \arg \min_{y, z, m} \frac{d_{ym}^2 + d_{zm}^2}{d_{yz}^2} \quad (13)$$

We can also add a term $\frac{|d_{ym} - d_{zm}|}{d_{yz}}$ which aids in balancing the lengths of the distance to each point.

4.2 Selecting Reference Points

Though all we need are 4 points in order to identify curvature, we are restricted by the fact that we have to find pairs with good surrogate midpoints. However, we will often observe many other potential locations which we can use for x . For example, it is very hard to elucidate curvature when x, y, z are nearly co-linear, and thus we would like triangles x, y, z which are closer to equilateral.

We exploit this by considering a scaled version of the triangle inequality. Let $C_\Delta \in [1, 2]$ be a constant which determines the flatness of the allowed triangles x, y, z . Then we select only the x such that

$$d_{ij} + d_{jk} \geq C_\Delta d_{ik} \quad \forall (i, j, k) \in (x, y, z). \quad (14)$$

We can estimate a single curvature by taking the median across the values of x . This tuning parameter allows us to pick the triangles closest to equilateral, which

tend to give the best estimates of the curvature. Letting $C_\Delta = 1$ allows for all triangles, no matter how flat they are and $C_\Delta = 2$ will only permit exact equilateral triangles. In practice we find that a value of $C_\Delta \in [1.05, 1.7]$ is effective and we set the default to be 1.3. Setting C_Δ to be too large results in no triangles found, and setting C_Δ too small will result in using triangles which are very flat, and often suffer from finite sample bias as well as high variance in their respective $\hat{\kappa}$ estimates. In practice, given a midpoint set y, z, m and a distance matrix \hat{D} we let $\mathbf{x} = \mathbf{x}(\hat{D}, C_\Delta)$ which are the points satisfying equation (14), then we can let $\hat{\kappa}_x = \kappa(\hat{D}, \mathbf{d}(x, y, z, m))$, and let $\hat{\kappa}_{med} = \text{median}\{\hat{\kappa}\}_{x \in \mathbf{x}}$. Given $\mathbf{x} := \mathbf{x}(C_\Delta, \hat{D}, y, z, m)$ we can construct the median estimator $\hat{\kappa}_{med, \mathbf{x}}$ of the curvature in equation (15).

$$\hat{\kappa}_{med, \mathbf{x}} = \text{median}_{x \in \mathbf{x}} \kappa(\hat{D}, y, z, m, x) \quad (15)$$

We can illustrate this phenomenon using the theoretical variance computed for the asymptotic results. In Figure 4 the smallest variance reference points in each of these curvatures are the ones that form nearly equilateral triangles with the reference points y, z . Additionally, the variance of the estimator tends to be larger in a given reference location as the curvature κ decreases.

Hence for a set $(y^{(j)}, z^{(j)}, m^{(j)})$ we can compute a set of estimates $\{\hat{\kappa}(y^{(j)}, z^{(j)}, m^{(j)})\}_{j=1}^J$ using all the x positions such that equation (14) is satisfied. If we wish to compute a single curvature estimate $\hat{\kappa}$ then a simple method will be to return the median over the set of estimates.

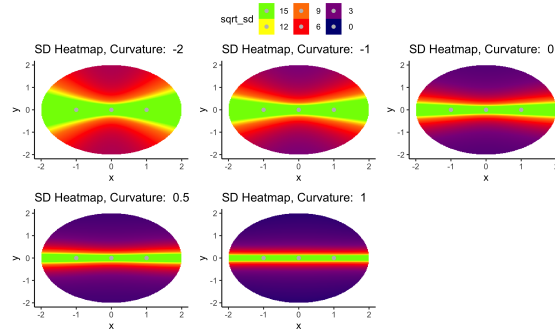


Figure 4: Variance as a function of x position. True points (y, m, z) in black.

4.3 Simulations

We construct a number of simulations in order to illustrate the performance of our curvature estimator, under the full model complexity. This will involve first sampling the parameters of a latent position cluster model to draw locations and variances independently, then sampling positions and random effects from the random latent position cluster model. This is to illustrate how even in the absence of a true placed, midpoint, that they will still occur from random draws. We simulate from the follow-

ing model:

$$\begin{aligned}
\mu_k &\sim F_{\mu}^{\mathcal{M}^p(\kappa)}(\mathbf{O}, R) & k &\in \{1, \dots, \lceil \sqrt{\rho} 50 \rceil\} \\
\sigma_k^2 &\sim F_{\sigma^2} & \boldsymbol{\pi} &\sim \text{Dirichlet}(\mathbf{2}) \\
\rho &\in \left\{ \frac{1}{\sqrt{2}}, 1, 2 \right\} & \kappa &\in \{-2, -1, -0.5, 0, 0.5, 1\}
\end{aligned}$$

where $F_{\mu}^{\mathcal{M}^p(\kappa)}(\mathbf{O}, R)$ denotes the prior distribution on the latent positions which is a uniform ball with radius R for $\kappa > 0$, and two concentric balls, one with radius R and the other with $R/2$ with equal probability for $\kappa \leq 0$. This setup facilitates forming midpoints since the volume of a ball grows exponentially as κ decreases. In all simulations, we set $R = 2.5$. This process determines a random latent position cluster model (LPCM). The locations of μ_k as well as the relative sizes of σ_k^2 determine where cliques are most likely to form in the latent space. The parameter ρ refers to the scale of the network, allowing for the number of centers to grow with ρ , $\boldsymbol{\pi}$ refers to the vector of cluster probabilities in the mixture model, $\boldsymbol{\mu}$ and $\boldsymbol{\sigma}^2$ refer to the cluster mean scale parameters and κ the true curvature of the space. The parameters $\boldsymbol{\mu}, \boldsymbol{\sigma}^2, \boldsymbol{\pi}$ determine a latent position cluster model, where the positions, $Z_i \sim F_Z := F_Z(\boldsymbol{\mu}, \boldsymbol{\sigma}^2, \boldsymbol{\pi}; \kappa)$. The mixture components correspond to the heat kernels in spherical space (Von-Mises Fischer distribution), Gaussian distribution in the Euclidean space, and the wrapped normal distribution in hyperbolic space [Nagano et al., 2019]. In all cases, let $p = 3$, so that we are also not forcing the positions to be drawn on a submanifold of dimension 2. The randomness the latent position cluster model incorporates the fact that we are not assigning good midpoints exactly, but finding them in the data each time we simulate a matrix. We let F_{σ^2} denote the gamma distribution with shape parameter $1/4^2$.

We then sample a random adjacency matrix A via the sampled LPCM

$$\begin{aligned}
n &= 5000\rho, & Z_i &\sim F_Z, & \nu_i &\sim F_{\nu, \rho} \\
p_{ij} &= \exp(\nu_i + \nu_j - d(Z_i, Z_j)) \\
A_{ij} &\sim \text{Bern}(p_{ij})
\end{aligned}$$

where $F_Z = F_Z(\boldsymbol{\pi}, \boldsymbol{\sigma}^2, \boldsymbol{\mu})$ is a particular draw of the random latent position cluster model. And $F_{\nu, \rho}$ is a trimmed normal distribution with mean -3ρ and standard deviation 3ρ trimmed at 0 and $\log(2/\sqrt{n})$ so that ν_i remain non-negative and to prevent isolated nodes. We let the minimum clique size used in the estimator be of size $\ell = (8 + 4 \log(\rho))$, which tends to generate 30-40 under this model. We set ℓ to be the minimum, but allow for cliques which are larger. We repeat this 500 times for each scale and curvature setting. For ease of computation, we find the cliques using the `maximal_cliques` function in the `igraph` R package [Csardi et al., 2006] clusters of the model. See Section F for additional graph statistics summaries over the simulations.

Figure 5 presents the results. We see that, as the clique size increases, we see a reduction in bias and variance. Also, the true curvature impacts the variance of the estimate at any particular sample size. This is for two reasons. Firstly, as we saw in Figure 4, the variance of the estimate is simply larger when κ is negative in nearly all regions of the space. Secondly, due to the vastness of the negatively curved spaces, we tend to have poorer quality midpoints form as well as fewer reference

points (x) which form good triangles which we can take medians across. In each of the simulations, we limit the number of cliques used in the estimator at 35 (50 for $\kappa \leq -1$) for computational convenience for numerous simulations; though in real data applications, this number can be larger in the practice. From the distance matrix, we compute the best midpoint set y, z, m according to equation (12) and compute the median of κ estimates for the x which satisfy equation (14) for $C_\Delta = 1.5$. We plot the results in Figure 5.

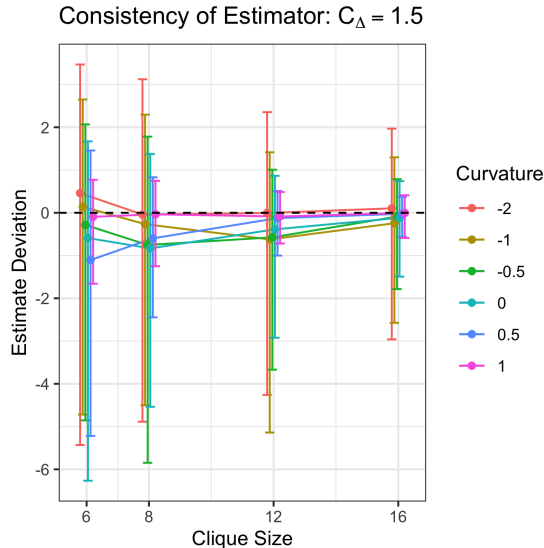


Figure 5: Consistency of Curvature Estimator. Upper error bars indicate 0.95 quantile of simulations and lower indicate 0.05 quantile. Central dots indicate the mean after trimming outliers larger than ± 100 (0.107% of the observations)

5 Application: Constant Curvature Test

A natural test one may wish to conduct is to verify whether a particular matrix can be embedded in a space of constant curvature

$$H_0 : \mathcal{M} = \mathcal{M}(\kappa).$$

This test could provide a model diagnostic (e.g. testing whether a latent variable model that assumes a single constant manifold is appropriate) or provide meaningful insights into heterogeneity in the structure of the graph.

In order to construct an appropriate test, we first consider a method of subsampling from the distribution of the cliques in order to approximate the distribution of the distance matrix estimate. This is based on the subsampling approach of Politis and Romano [1994], which can be used to approximate the distribution of a random variable via subsampling under conditions weaker than the bootstrap, similar to the strategy in Lubold et al. [2023]. This is highlighted in Algorithm 1. For simplicity, we illustrate the algorithm with the subsampling rate $b = \frac{\ell-1}{\ell}$ where ℓ is the smallest clique size.

Let $\mathcal{I} = \{\mathbf{I}_k\}_{k=1}^K$ denote a set of indices corresponding to cliques for which $\mathbf{I}_k \cap \mathbf{I}_{k'} = \emptyset$ when $k \neq k'$. Let $\widehat{\nu}_{\mathbf{I}_k}$ denote the set of random effects indexed by \mathbf{I}_k . In

Algorithm 1 Subsample Distribution of \widehat{D}

Require: $G, B \geq 1$ and $\{\mathbf{I}_k\}_{k=1}^K$

- 1: **for** $b \in \{1, 2, \dots, B\}$ **do**
 - 2: **for** $k \in \{1, 2, \dots, K\}$ **do** Sample $|\mathbf{I}_k| - 1$ nodes without replacement from \mathbf{I}_k and denote this set $\mathbf{I}_k^{(b)}$
 - 3: **end for**
 - 4: Denote the set $\mathcal{I}^{(b)} = \{\mathbf{I}_k^{(b)}\}_{k=1}^K$
 - 5: Let $\nu^{(b)} = \nu_{\mathcal{I}^{(b)}}$ denote the corresponding random effects estimates.
 - 6: Let $\widehat{D}_0^{(b)} = f_0(A, \mathcal{I}^{(b)}, \nu^{(b)})$ Initial Consistent estimate
 - 7: Let $\widehat{D}_1^{(b)} = f_1(\widehat{D}_0^{(b)}; A, \mathcal{I}^{(b)}, \nu^{(b)})$ One-step Estimate
 - 8: **end for**
 - 9: **return** $\{\widehat{D}^{(b)}\}_{b=1}^B = \{\widehat{D}_1^{(b)}\}_{b=1}^B$
-

Algorithm 1 f_0 denotes the distance estimation by the method of Lubold et al. [2023] and sparse modification of the distances via the Floyd Warshall Algorithm so that \widehat{D}_0 is a metric. This is known as a sparse metric repair problem [Gilbert and Jain, 2017]. For full details, see the appendix Section B.2. The subsequent step f_1 simply is a short-hand for applying the one-step estimation procedure of equation (11).

For a distance matrix D , let $\kappa_u(D; y, z, m, x)$ and $\kappa_l(D; y, z, m, x)$ denote the upper and lower bound indexed by a set y, z, m, x . Where y, z, m are the endpoints and midpoints, and x is a reference point. Given a set of samples of a distance matrices $\{\widehat{D}^{(b)}\}_{b=1}^B$ and a set of midpoint sets $y^{(j)}, z^{(j)}, m^{(j)}$ with corresponding reference points $\mathbf{x}^{(j)}$, we can test whether the curvature is constant between these regions $j \in \{1, 2, \dots, J\}$:

$$H_0 : \kappa_j = \kappa_{j'} \text{ for all } j, j' \in \{1, 2, \dots, J\}$$

using Algorithm 2.

The constant curvature test takes a subsample of the distance matrices $\{\widehat{D}\}_{b=1}^B$ generated from Algorithm 1, and a set of midpoints and reference points $\{y^{(j)}, z^{(j)}, m^{(j)}, \mathbf{x}^{(j)}\}_{j=1}^J$ to estimate the upper and lower bounds on the curvature. In practice, each set $\mathbf{x}^{(j)}$ can be selected by the triangle filtering method of equation (14). To reduce the variance of the estimates, we take the median across regions at each x and we take the minimum of the upper bounds, (and maximum of the lower bounds) to bound the corresponding distance matrix. We repeat this over the set of $b \in \{1, 2, \dots, B\}$ estimates of the curvature, bounds and assess the subsampled quantiles of the total upper and lower bounds. We lastly find the corresponding minimum quantile for which there is a separation between these sampled bounds and return that as the p -value for the subsampled constant curvature test.

5.1 Simulations

Under the same simulation setup as in Section 4.3 we can illustrate the coverage of the constant curvature test as a function of clique size. Due to computational complexity, we reduce this to a maximum clique size of 12. We see in Figure 6 that this

Algorithm 2 Constant Curvature Test

Require: $\{\widehat{D}^{(b)}\}_{b=1}^B$ and $\{y^{(j)}, z^{(j)}, m^{(j)}, \mathbf{x}^{(j)}\}_{j=1}^J$

- 1: **for** $b \in \{1, 2, \dots, B\}$ **do**
- 2: **for** $j \in \{1, 2, \dots, J\}$ **do**
- 3: **for** $x \in \{\mathbf{x}^{(j)}\}$ **do**
- 4: $\widehat{\kappa}_{u,x}^{(b,j)} = \kappa_u(\widehat{D}^{(b)}; y^{(j)}, z^{(j)}, m^{(j)}, x)$
- 5: $\widehat{\kappa}_{l,x}^{(b,j)} = \kappa_l(\widehat{D}^{(b)}; y^{(j)}, z^{(j)}, m^{(j)}, x)$
- 6: **end for**
- 7: Compute $\widehat{\kappa}_u^{(b,j)} = \text{median}_{x \in \mathbf{x}^{(j)}} \widehat{\kappa}_{u,x}^{(b,j)}$
- 8: Compute $\widehat{\kappa}_l^{(b,j)} = \text{median}_{x \in \mathbf{x}^{(j)}} \widehat{\kappa}_{l,x}^{(b,j)}$
- 9: **end for**
- 10: Compute $\widehat{\kappa}_u^{(b)} = \min_{j \in \{1, 2, \dots, J\}} \widehat{\kappa}_u^{(b,j)}$
- 11: Compute $\widehat{\kappa}_l^{(b)} = \max_{j \in \{1, 2, \dots, J\}} \widehat{\kappa}_l^{(b,j)}$
- 12: **end for**
- 13: Let $\widehat{\kappa}_{u,(m)}$ be the m^{th} order statistic of $\{\widehat{\kappa}_u^{(b)}\}_{b=1}^B$
- 14: Let $\widehat{\kappa}_{l,(m)}$ be the m^{th} order statistic of $\{\widehat{\kappa}_l^{(b)}\}_{b=1}^B$
- 15: Let $m = \min\{m : \widehat{\kappa}_{u,(m)} \geq \widehat{\kappa}_{l,(B-m)}\}$
- 16: **return** p -value: $\min\{2m/B, 1\}$

test tends to be overly conservative in small sample sizes, but returns to nearly nominal coverage when cliques are larger. This is due to the fact that a poor quality midpoint leads to more conservative bounds of κ_l, κ_u , however, this can be improved with better aligning midpoints.

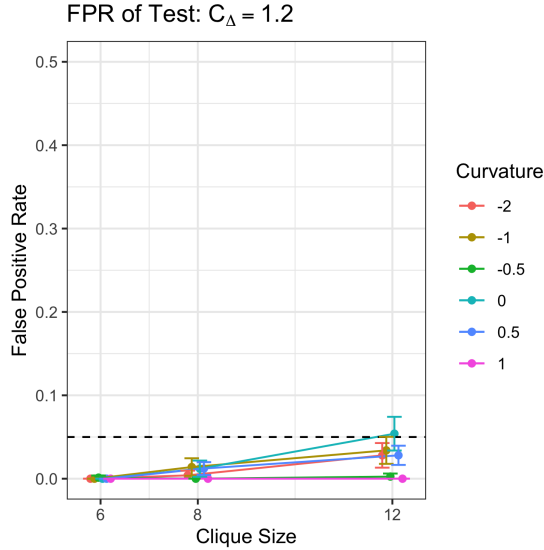


Figure 6: False positive rate for constant curvature test.

5.2 Multiplex Network Constant Curvature Tests.

In this next simulation, we consider a model of multiplex (or multiview) networks. Several methods exist for modelling multiplex networks via extensions of the latent distance model, however, most assume the same geometry latent space among views Salter-Townshend and McCormick [2017], MacDonald et al. [2022]. For example, Salter-Townshend and McCormick [2017] model the multiple relationships between individuals in the Banerjee et al. [2013] diffusion of microfinance dataset using Euclidean spaces. We illustrate a simulated example where this is not the case, and how our method can be used to detect this.

We first construct a latent position model for which multiple views are drawn from a common set of latent positions, however, these positions are common coordinates of spheres of curvature $(\kappa_1, \kappa_2) = (0.5, 1.5)$ respectively. Additional details for the simulation are identical to the consistency simulations in Section 4.3.

In this case for a set of latent positions, we simulate a multiplex network for which latent spherical positions are the same for this network set, however, they are embedded in two spheres of different radii and thus different curvatures. We simulate 200 pairs of network and test the curvature difference and plot the power in Figure 7. In each view we compute the optimal midpoint set $y^{(r)}, z^{(r)}, m^{(r)}$ from each view’s distance matrix $\widehat{D}^{(1)}$ or $\widehat{D}^{(2)}$ via equation 13 and subsample each distance matrix separately, and concatenate them to conduct the constant curvature test. In Figure 7 we see that the power of the least grows with the clique size.

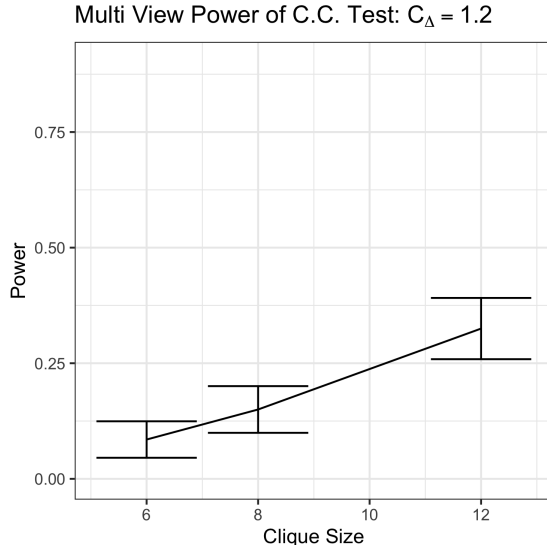


Figure 7: Power of constant curvature of multiview.

5.3 Noncanonical manifolds

We next illustrate the ability of our method to detect non-constant curvature within the latent space. Since many common latent space models are constantly curved by assumption, it is of interest to verify whether this agrees with the observed data.

Though the sphere, the hyperbolic and Euclidean spaces all have closed form solutions for their distances, this is not true of arbitrary manifolds, and we highlight our example on one which allows us to compute these distances.

We construct a latent space consisting of two adjacent spheres. For any two points in the same sphere the distance is straightforward to compute. For any two points (x, y) in opposite spheres, the distance can be computed via the distance to the origin $(1, 0, 0)$ in each of the spheres. This is due to the fact any geodesic must pass through the connecting point, i.e. the origin.

$$d_{\mathcal{M}}(x, y) = d_1(x, o) + d_2(o, y)$$

For these simulations, our manifold consists of two adjacent spheres of curvature $\kappa_1 = 1, \kappa_2 = 1.5$ respectively. This manifold was chosen as distances were straightforward to compute but also does not contain a constant curvature. The latent cluster locations are sampled via uniforms centered on opposite poles. We again simulate 200 draws from the latent position cluster model and test for constant curvature by finding the best three non-overlapping sets minimizing equation (13). We plot the corresponding power in Figure 8 which again increases as the clique size increases.

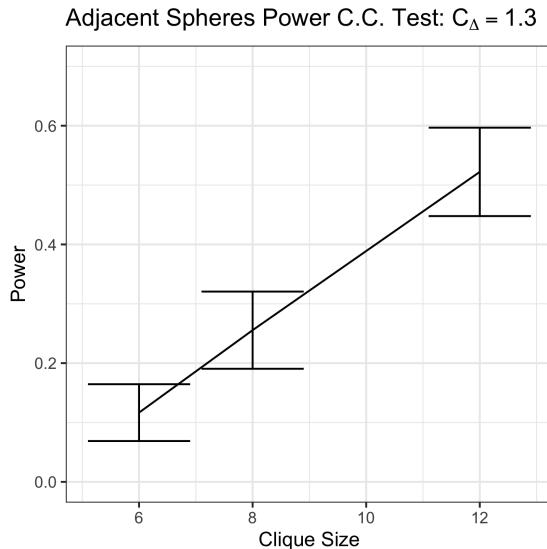


Figure 8: Constant Curvature Test Power: Adjacent Spheres.

5.4 Geometry of Coauthorship

We consider the sets of co-authorship networks introduced in Leskovec et al. [2007]. These consist of citation networks from High Energy Particle Physics, General Relativity, Astrophysics, and Condensed Matter Physics, with sizes of each of the networks seen in Table 1. These networks consist of authors as nodes where an edge exists whether any pair of authors has co-authored a paper on ArXiv in any of the specified subject areas between 1993 and 2003. When these data were collected, these were the top 5 most common subject areas in Physics.

In previous machine learning applications, hyperbolic network embeddings have been successful in tasks such as link-prediction or node in citation networks [Nickel and Kiela, 2017, Chami et al., 2019, Chamberlain et al., 2017]. This is due to the fact that the hierarchical structure (tree-like) structure generally can be more easily embedded in a negatively curved space. We wish to answer the question of, under a latent space assumption, is the data generated from a space of constant curvature?

Physics Sub-field	Number of Nodes (n)	Number of Edges ($ E $)
Astrophysics	18771	396160
Condensed Matter Physics	23133	186936
General Relativity	5241	28980
High Energy Particle Physics	12006	237010
High Energy Particle Physics (Theory)	9875	51971

Table 1: Physics Co-authorship network sizes.

For each of these networks, we construct an estimate of the distance matrix with random effects, followed by an estimate of the curvature. For each of these, we use a triangle filtering constant $C_{\Delta} = 1.2$ and a minimum clique size seen in Table 2. We lastly apply our test to see if the difference in curvature is present across the networks.

Physics Sub-field	Min Clique Size (ℓ)	Number of Cliques of Size $\geq \ell$ (K)	Largest Clique Size
Astrophysics	19	57	57
Condensed Matter Physics	12	52	26
General Relativity	7	44	44
High Energy Particle Physics	14	42	239
High Energy Particle Physics (Theory)	7	42	32

Table 2: Clique size and number of cliques used to estimate distance matrix.

We estimate the curvature, at the best midpoint set for each of the networks, along with the following p-values for tests of whether a network has constant curvature.

We see that Astrophysics and General Relativity are estimated to have a large negative curvature, which however, may not be constant in the case of the Astrophysics citation network. In the Astrophysics network, at the best 3 midpoint sets, we estimate curvature to be $(-0.01378, -\infty, 0.306)$. The estimate of $-\infty$ comes from the fact there is a minimum distance of d_{xm} given the other 3, d_{xy}, d_{yz}, d_{xz} , and since the midpoints are not exact, sometimes this length can be too short to embed in any of the hyperbolic spaces. If the estimated distance is below this value we call the estimate $-\infty$, and similarly ∞ if it is too large. This highlights the fact that this network appears to have negatively curved, positively curved and flat regions, and therefore models which reflect only a single curvature, may not capture the individual level behavior of the network very well. In contrast, condensed matter physics

Physics Sub-field	Curvature Estimate	Constant Curve Test p-value
Astrophysics	-0.01378	0.030
Condensed Matter Physics	0.107	1.000
General Relativity	0.0989	1.000
High Energy Particle Physics	-0.986	1.000
High Energy Particle Physics (Theory)	0.1674	0.240

Table 3: Curvature estimates from best midpoints and p-values for constant curvature test $J = 3$.

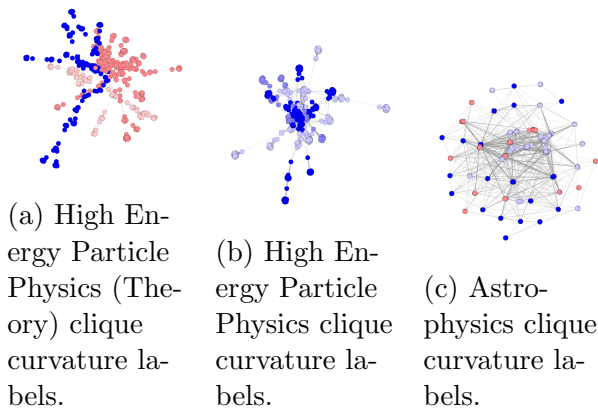


Figure 9: Cliques Colored to nearest labeled curvature value. Blue, negative and red positive, with p values of constant curvature decreasing from left to right.

and HEP physics seem to have a slight curvature, though both are nearly flat networks.

6 Application: Multiple change point detection

Another natural question one may seek to answer is whether a change in latent curvature has occurred and being able to distinguish this from changes in latent positions. Standard Gaussian multiple change point algorithms (for example that of Harchaoui and Lévy-Leduc [2010]) are not immediately well-suited to this problem due to the possibility of large outliers.

We apply the method of Fearnhead and Rigaiil [2016] which proposes a multiple changepoint detection algorithm under the presence of outliers. For a particular network, we may measure a collection of estimates of the curvature $\{\hat{\kappa}_t\}_{t=1}^T$. Under this model, we assume that a network has a constant curvature within a single time point

t. We construct an objective function for the changepoint problem

$$L(\theta) = \sum_{t=1}^T \tilde{\ell}(\hat{\kappa}_t, \theta_t)$$

In our application, we let $\tilde{\ell}$ be the biweight loss, however, more general loss functions such as absolute deviation or Huber also available (see Fearnhead and Rigaiil [2016] for a more in depth discussion of robust change point detection). In multiple change point detection algorithms a penalty of β for the number of segments included is also applied. Let $J(\theta)$ denote a function of the number of breaks in the sequence θ . Then the full loss function is

$$L(\theta; \beta) = L(\theta) + \beta J(\theta). \tag{16}$$

In our setting, since we tend to have large negative outliers, we also apply the $c \tanh(\cdot/c)$ function which smoothly truncates the extreme values. In all simulations and applications where this is applied, we set $c = 10$.

We next apply this to a simulation setting where we construct a sequence of networks with latent positions.

$$Z_i^{(t)} = \mathcal{F}(Z_i^{(t-1)}, \epsilon_i^{(t)})$$

where $Z_{(t-1)i}$ is the location's previous position, $\epsilon_i^{(t)}$ is a noise random variable sampled from the true cluster's density, and \mathcal{F} stands for the mean on the sphere (the Fréchet mean). We set three different curvatures

$$\kappa_1 = 1.0 \quad \kappa_2 = 0.15 \quad \kappa_3 = 1.3$$

with time changes at $t_1 = 18, t_2 = 35$ and total time $T = 50$.

As illustrated before, we use the `robseg` package introduced in Fearnhead and Rigaiil [2016] and use the absolute value loss. We see that as ℓ increases, we are able to consistently estimate the true curvature function. We plot the mean of the absolute deviation of the curvature estimate over 200 simulations as a function of the clique size using the default tuning parameter from the `Robseg` R package. We plot the results in Figure 10 showing consistency of the true curvature with respect to the mean absolute deviation.

6.1 LANL Netflow and Changepoint detection

For our second application, we apply our estimates of network curvature to Los Alamos Unified Network and Host Dataset, and illustrate that changes in curvature can be used to identify a red team attack. A red team attack is a planned exercise by cybersecurity team that infiltrates a device network as a test of network security.

This dataset consists of 89 days of directed communication events between $n = 27436$ devices in the Los Alamos National Laboratory. The dataset consists of 56 normal days followed by a red team attack beginning on day 57 and continuing to day 89.

Anomaly detection is of great interest for many cybersecurity applications and recently latent space models have been shown to be a promising avenue of detecting

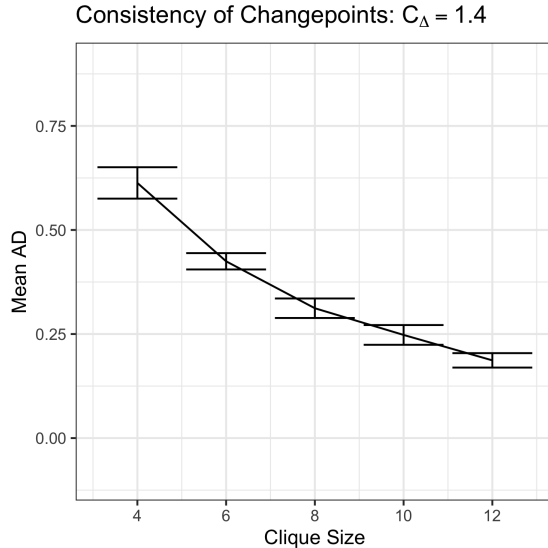


Figure 10: Mean absolute deviation of curvature estimates over time window=.

changes in node properties [Lee et al., 2019]. We take a different approach and illustrate how changepoint methods can be applied to sequential estimates of curvature in this dataset, highlighting the role of curvature as a summary of network behavior.

We consider a dataset preprocessed in the same manner as in Lee et al. [2019]. Edges are defined in this dataset as messages passed between nodes during a particular time period. In order to maintain enough connections to find cliques, we consider a connection to be formed if any message was passed in the previous 4 days. We then compute the curvature values at each time point and take the median over the time-point. We scale each estimated value by $c \tanh(\cdot/c)$ for $c = 10$ in order to limit the influence of extreme negative outliers. We then apply the off the shelf change point algorithm of Fearnhead and Rigaiil [2016]. Using a $C_{\Delta} = 1.4$ we estimate the curvature at each time frame. We consider a minimum clique size of $\ell = 5$. Due to the small number of available cliques, and relative sparsity of the dataset, we restrict the random effects to be 0 and compute the corresponding distance matrix.

In Figure 11 we show that the most substantial changepoint in curvature occurs at the time of the red team attack. In contrast, these changes are much less substantial in Figure 12 when using simple graph motifs from the daily averages.

Since the time of detection after the event is most important, we wish to investigate the time after detection as a function of the number of events involved (alarm rate). We show that in Figure 13 that our method achieves a much smaller detection delay given any alarm rate.

This suggests that models accounting for changes in network curvature may be a promising avenue for the development of specialized models to detect anomalous events in the online setting.

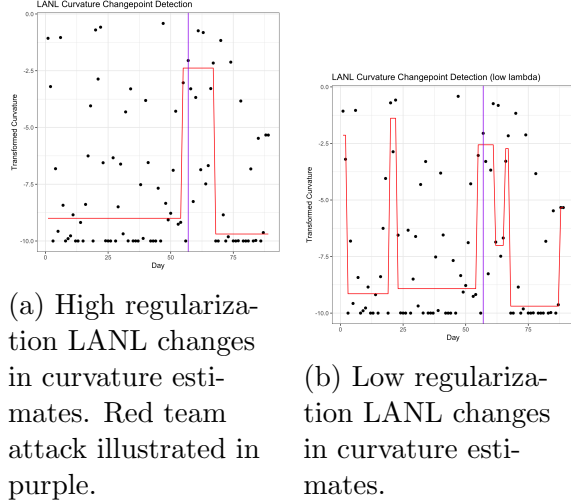


Figure 11: Two regularization values for LANL Netflow changepoint. Red team attack illustrated in purple.

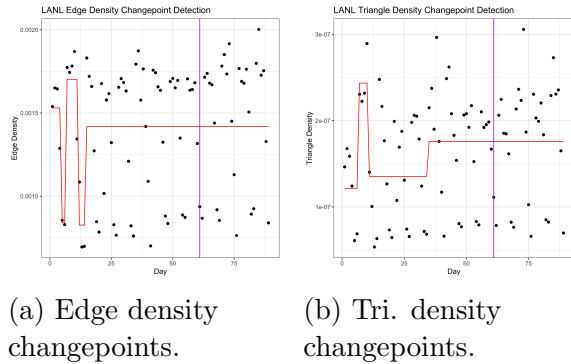


Figure 12: Changepoints of daily LANL measurements using simple graph motifs. Red team attack illustrated in purple.

7 Discussion

Riemannian sectional curvature is a fundamental property of a manifold, and we present a novel method to estimate it from a noisy distance matrix. Though our motivating example involves estimating the distances of a latent distance model from a random network, the curvature estimates (and constant curvature tests) in this paper are more general and can be applied whenever one can either estimate a distance matrix (or bootstrap or sub-sample their distance matrices).

Though in our method one may worry about selection effects, given that we choose a midpoint from the data. However, since we do not select for large or small curvature, therefore selection effects are of minor concern. Another concern may be the quality of midpoints found in real data. In practice, we find good midpoints can be found in our real datasets. For example, the midpoint minimization equation (12) which has a value at the true midpoint of 0.5 were found to be 0.5000003, 0.5039, 0.50049, 0.50012, 0.50043 in the best midpoints of the 5 physics co-authorship net-

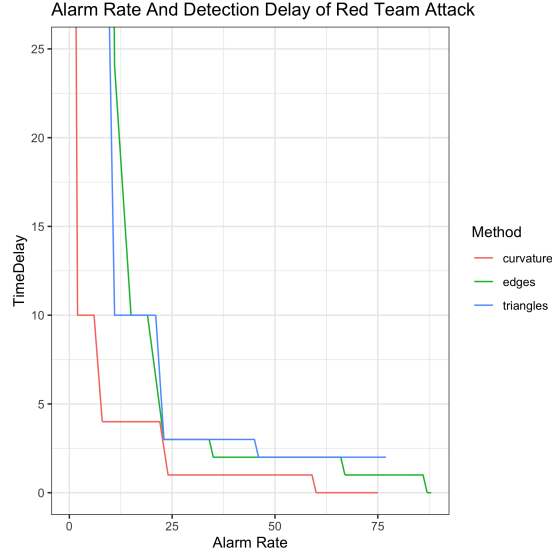


Figure 13: Time to first changepoint in days (TimeDelay) as a function of Alarm Rate.

works respectively, suggesting we have near midpoints occurring in real data.

Though we develop a test for detecting whether the curvature is constant on the latent manifold, a natural open question is what should a practitioner do if they find that their data are not represented well by this model. One might instead use non-geometric models such as stochastic block models and their variants, however, this also suggests the development of latent distance models which are not restricted to constant curvature.

The development of such a model class as something which will scale to large networks is of further interest. Computing gradients on arbitrary Riemannian manifolds may prove to be challenging when the positions are in fact latent. One promising approach we plan to investigate in future work is that of product spaces for latent space models. This geometry has seen considerable success in representation learning tasks such as Gu et al. [2018] or Zhang et al. [2021].

One may consider the interpretation of the curvature parameter κ when a set of points does not lie within a canonical manifold. Our method merely fits for each (x, y, z, m) the particular constant curvature manifold, which will embed these 4 distances, and taking the median will estimate the median of the curvatures of these interpolating spaces. This idea is reminiscent of the manifold learning methods of Li et al. [2017], Li and Dunson [2019] which use spherelets to approximate manifolds rather locally linear approximations of tangent spaces.

When considering the unified network and flow dataset from LANL, we must transform the original dataset of pairs of individuals and times to one which considers a set of graphs over time. A more realistic model for the data-generating mechanism may be one related to a Poisson process (or other point processes) with intensity parameters $\mu_{ij,t} \propto -d_{ij,t}$.

Future extensions may include methods for fitting models in the product space geometry (as is done in Gu et al. [2018]) as well as movement towards statistically consistent node-level definitions of network curvature as well as more application-focused development of anomaly detection incorporating curvature into the models.

8 Competing interests

No competing interest is declared.

9 Acknowledgments

The authors would like to thank Marina Meila, Shane Lubold, Adam Visokay and Abel Rodriguez for their valuable suggestions. Research reported in this publication was supported by the National Institute Of Mental Health of the National Institutes of Health under Award Number DP2MH122405 and the National Science Foundation under grant NSF SES-2215369. Partial support for this research came from a Eunice Kennedy Shriver National Institute of Child Health and Human Development research infrastructure grant, P2C HD042828, to the Center for Studies in Demography and Ecology at the University of Washington. Funding was also provided by the National Science Foundation under grant NSF SES-2215369.

References

- E. Aliverti and D. Durante. Spatial modeling of brain connectivity data via latent distance models with nodes clustering. *Statistical Analysis and Data Mining: The ASA Data Science Journal*, 12(3):185–196, 6 2019. ISSN 1932-1872. doi: 10.1002/SAM.11412. URL <https://onlinelibrary.wiley.com/doi/full/10.1002/sam.11412>.
- E. B. Andersen. Asymptotic properties of conditional maximum-likelihood estimators. *Journal of the Royal Statistical Society: Series B (Methodological)*, 32(2): 283–301, 1970.
- E. D. Andersen and K. D. Andersen. The mosek interior point optimizer for linear programming: an implementation of the homogeneous algorithm. In *High performance optimization*, pages 197–232. Springer, 2000.
- A. Banerjee, A. G. Chandrasekhar, E. Duflo, and M. O. Jackson. The Diffusion of Microfinance. *Science*, 341(6144), 2013. ISSN 10959203. doi: 10.1126/SCIENCE.1236498.
- V. Barkanass, U. Jost, and E. Hancock. Geometric sampling of networks. *Journal of Complex Networks*, 10(4), 6 2022. ISSN 2051-1310. doi: 10.1093/COMNET/CNAC014. URL <https://academic.oup.com/comnet/article/10/4/cnac014/6644814>.
- D. S. Bassett, P. Zurn, and J. I. Gold. On the nature and use of models in network neuroscience. *Nature Reviews Neuroscience 2018 19:9*, 19(9):566–578, 7 2018. ISSN 1471-0048. doi: 10.1038/s41583-018-0038-8. URL <https://www.nature.com/articles/s41583-018-0038-8>.
- E. Begelfor and M. Werman. The World is not always Flat or Learning Curved Manifolds. *School of Engineering and Computer Science, Hebrew University of Jerusalem., Tech. Rep*, 3(8), 2005.

- M. Berger. An extension of rauch’s metric comparison theorem and some applications. *Illinois Journal of Mathematics*, 6(4):700–712, 1962.
- L. M. Blumenthal and B. E. Gillam. Distribution of Points in n-Space. *The American Mathematical Monthly*, 50(3):181, 3 1943. ISSN 00029890. doi: 10.2307/2302400.
- S. P. Borgatti, A. Mehra, D. J. Brass, and G. Labianca. Network analysis in the social sciences. *Science*, 323(5916):892–895, 2 2009. ISSN 00368075. doi: 10.1126/SCIENCE.1165821/ASSET/2421E2F8-2DC7-4CAD-8A84-471B43A3C443/ASSETS/GRAPHIC/323.892_F5.JPEG. URL <https://www.science.org/doi/10.1126/science.1165821>.
- J. S. Brauchart, A. B. Reznikov, E. B. Saff, I. H. Sloan, Y. G. Wang, and R. S. Womersley. Random Point Sets on the Sphere — Hole Radii, Covering, and Separation. *Experimental Mathematics*, 27(1):62–81, 12 2015. ISSN 1944950X. doi: 10.1080/10586458.2016.1226209. URL <https://arxiv.org/abs/1512.07470v2>.
- R. S. Burt. *Structural holes: The social structure of competition*. Harvard University Press, Cambridge, MA, 1992.
- V. Buskens and A. Van de Rijt. Dynamics of networks if everyone strives for structural holes. *American Journal of Sociology*, 114(2):371–407, 2008.
- T. Cai, J. Fan, and T. Jiang. Distributions of Angles in Random Packing on Spheres. *Journal of Machine Learning Research*, 14:1837–1864, 2013.
- B. P. Chamberlain, J. R. Clough, and M. P. Deisenroth. Neural Embeddings of Graphs in Hyperbolic Space. In *13th international workshop on mining and learning from graphs held in conjunction with KDD*, 2017.
- I. Chami, R. Ying, C. Ré, and J. Leskovec. Hyperbolic Graph Convolutional Neural Networks. *Advances in Neural Information Processing Systems*, 32, 10 2019. ISSN 10495258. doi: 10.48550/arxiv.1910.12933. URL <https://arxiv.org/abs/1910.12933v1>.
- G. Csardi, T. Nepusz, et al. The igraph software package for complex network research. *InterJournal, complex systems*, 1695(5):1–9, 2006.
- F. Durante, J. Fernández-Sánchez, and C. Sempì. A topological proof of Sklar’s theorem. *Applied Mathematics Letters*, 26(9):945–948, 9 2013. ISSN 0893-9659. doi: 10.1016/J.AML.2013.04.005.
- H. Farooq, Y. Chen, T. T. Georgiou, A. Tannenbaum, and C. Lenglet. Network curvature as a hallmark of brain structural connectivity. *Nature Communications* 2019 10:1, 10(1):1–11, 10 2019. ISSN 2041-1723. doi: 10.1038/s41467-019-12915-x. URL <https://www.nature.com/articles/s41467-019-12915-x>.
- P. Fearnhead and G. Rigai. Changepoint Detection in the Presence of Outliers. *Journal of the American Statistical Association*, 114(525):169–183, 9 2016. ISSN 1537274X. doi: 10.48550/arxiv.1609.07363. URL <https://arxiv.org/abs/1609.07363v2>.

- B. K. Fosdick, T. H. McCormick, T. B. Murphy, T. L. J. Ng, and T. Westling. Multiresolution network models. *Journal of Computational and Graphical Statistics*, 28(1):185–196, 8 2016. ISSN 15372715. doi: 10.48550/arxiv.1608.07618. URL <https://arxiv.org/abs/1608.07618v5>.
- M. Frechet. Sur la distance de deux lois de probabilite. *CR. Acad Sci. Paris*, 244, 1957.
- A. Fu, B. Narasimhan, and S. Boyd. CVXR: An R package for disciplined convex optimization. *Journal of Statistical Software*, 94(14):1–34, 11 2020. ISSN 15487660. doi: 10.18637/jss.v094.i14. URL <https://CRAN.R-project>.
- S. Gallot, D. Hulin, and J. Lafontaine. *Riemannian Geometry*. Universitext. Springer Berlin Heidelberg, Berlin, Heidelberg, 2004. ISBN 978-3-540-20493-0. doi: 10.1007/978-3-642-18855-8. URL <http://link.springer.com/10.1007/978-3-642-18855-8>.
- A. C. Gilbert and L. Jain. If it ain’t broke, don’t fix it: Sparse metric repair. In *2017 55th Annual Allerton Conference on Communication, Control, and Computing (Allerton)*, pages 612–619. IEEE, 2017.
- M. Gromov, editor. *Metric Structures for Riemannian and Non-Riemannian Spaces*. Birkhäuser Boston, 2007. doi: 10.1007/978-0-8176-4583-0.
- A. Gu, F. Sala, B. Gunel, and C. Ré. Learning mixed-curvature representations in product spaces. In *International Conference on Learning Representations*, 2018.
- Z. Harchaoui and C. Lévy-Leduc. Multiple change-point estimation with a total variation penalty. *Journal of the American Statistical Association*, 105(492):1480–1493, 2010.
- W. Hoeffding. Masstabvariante Korrelationstheorie. *Schriftl Math. Inst. Univ. Berlin*, 5(6), 1940.
- P. D. Hoff, A. E. Raftery, and M. S. Handcock. Latent space approaches to social network analysis. *Journal of the American Statistical Association*, 97(460):1090–1098, 2002.
- W. Killing. Ueber die Clifford-Klein’schen Raumformen. *Mathematische Annalen 1891 39:2*, 39(2):257–278, 6 1891. ISSN 1432-1807. doi: 10.1007/BF01206655. URL <https://link.springer.com/article/10.1007/BF01206655>.
- W. Klingenberg. *Riemannian Geometry*. Walter de Gruyter, 1 edition, 12 1995. doi: 10.1515/9783110905120.
- L. Le Cam. On the asymptotic theory of estimation and testing hypotheses. In *Proceedings of the Third Berkeley Symposium on Mathematical Statistics and Probability, Volume 1: Contributions to the Theory of Statistics*, volume 3, pages 129–157. University of California Press, 1956.

- W. Leal, G. Restrepo, P. F. Stadler, and J. Jost. Forman-Ricci Curvature for Hypergraphs. *Advances in Complex Systems*, 24(1), 11 2018. doi: 10.13140/RG.2.2.27347.84001. URL <http://arxiv.org/abs/1811.07825><http://dx.doi.org/10.13140/RG.2.2.27347.84001>.
- W. Lee, T. H. McCormick, J. Neil, M. Cole, S. Microsoft, and Y. Cui. Anomaly Detection in Large Scale Networks with Latent Space Models. *Technometrics*, pages 1–23, 11 2019. ISSN 0040-1706. doi: 10.1080/00401706.2021.1952900. URL <https://arxiv.org/abs/1911.05522v2>.
- J. Leskovec, J. Kleinberg, and C. Faloutsos. Graph evolution. *ACM Transactions on Knowledge Discovery from Data (TKDD)*, 1(1), 3 2007. ISSN 15564681. doi: 10.1145/1217299.1217301. URL <https://dl.acm.org/doi/abs/10.1145/1217299.1217301>.
- D. Li and D. B. Dunson. Geodesic distance estimation with spherelets. *arXiv preprint arXiv:1907.00296*, 2019.
- D. Li, M. Mukhopadhyay, and D. B. Dunson. Efficient manifold and subspace approximations with spherelets. *arXiv preprint arXiv:1706.08263*, 2017.
- T. Lok, J. Ng, T. B. Murphy, T. Westling, T. H. McCormick, and B. Fosdick. Modeling the social media relationships of Irish politicians using a generalized latent space stochastic blockmodel. *Annals of Applied Statistics*, 15(4):1923–1944, 12 2021. ISSN 1932-6157. doi: 10.1214/21-AOAS1483.
- S. Lubold, A. G. Chandrasekhar, and T. H. McCormick. Identifying the latent space geometry of network models through analysis of curvature. *Journal of the Royal Statistical Society Series B: Statistical Methodology*, 2023.
- P. W. MacDonald, E. Levina, and J. Zhu. Latent space models for multiplex networks with shared structure. *Biometrika*, 109(3):683–706, 2022.
- Y. Nagano, S. Yamaguchi, Y. Fujita, and M. Koyama. A Wrapped Normal Distribution on Hyperbolic Space for Gradient-Based Learning. *36th International Conference on Machine Learning, ICML 2019, 2019-June:8242–8251*, 2 2019. doi: 10.48550/arxiv.1902.02992. URL <https://arxiv.org/abs/1902.02992v2>.
- C. C. Ni, Y. Y. Lin, F. Luo, and J. Gao. Community Detection on Networks with Ricci Flow. *Scientific Reports 2019 9:1*, 9(1):1–12, 7 2019. ISSN 2045-2322. doi: 10.1038/s41598-019-46380-9. URL <https://www.nature.com/articles/s41598-019-46380-9>.
- M. Nickel and D. Kiela. Poincaré Embeddings for Learning Hierarchical Representations. *Advances in Neural Information Processing Systems*, 30, 2017.
- Y. Ollivier. Ricci curvature of Markov chains on metric spaces. *Journal of Functional Analysis*, 256(3):810–864, 1 2007. ISSN 00221236. doi: 10.48550/arxiv.math/0701886. URL <https://arxiv.org/abs/math/0701886v4>.

- L. Papadopoulos, M. A. Porter, K. E. Daniels, and D. S. Bassett. Network analysis of particles and grains. *Journal of Complex Networks*, 6(4):485–565, 8 2018. ISSN 20511329. doi: 10.1093/COMNET/CNY005. URL <https://academic.oup.com/comnet/article/6/4/485/4959635>.
- X. Pennec. Probabilities and statistics on Riemannian manifolds: Basic tools for geometric measurements. In *International Workshop on Nonlinear Signal and Image Processing*, pages 194–198, Antalya, Turkey, 6 1999. URL <http://www-sop.inria.fr/epidaure/personnel/pennec/pennec.html>.
- D. N. Politis and J. P. Romano. Large Sample Confidence Regions Based on Sub-samples under Minimal Assumptions. <https://doi.org/10.1214/aos/1176325770>, 22 (4):2031–2050, 12 1994. ISSN 0090-5364. doi: 10.1214/AOS/1176325770.
- M. Salter-Townshend and T. H. McCormick. Latent space models for multi-view network data. *Annals of Applied Statistics*, 11(3):1217–1244, 9 2017. ISSN 1932-6157. doi: 10.1214/16-AOAS955. URL <https://projecteuclid.org/journals/annals-of-applied-statistics/volume-11/issue-3/Latent-space-models-for-multiview-network-data/10.1214/16-AOAS955.full>.
- A. Samal, H. K. Pharasi, S. J. Ramaia, H. Kannan, E. Saucan, J. Jost, and A. Chakraborti. Network geometry and market instability. *Royal Society Open Science*, 8(2), 2 2021. ISSN 20545703. doi: 10.1098/RSOS.201734. URL <https://royalsocietypublishing.org/doi/10.1098/rsos.201734>.
- R. Sandhu, T. Georgiou, E. Reznik, L. Zhu, I. Kolesov, Y. Senbabaoglu, and A. Tannenbaum. Graph Curvature for Differentiating Cancer Networks. *Nature Scientific Reports*, 5(1):1–13, 7 2015. ISSN 2045-2322. doi: 10.1038/srep12323. URL <https://www.nature.com/articles/srep12323>.
- R. S. Sandhu, T. T. Georgiou, and A. R. Tannenbaum. Ricci curvature: An economic indicator for market fragility and systemic risk. *Science Advances*, 2(5), 5 2016. ISSN 23752548. doi: 10.1126/SCIADV.1501495/SUPPL_FILE/1501495.SM.PDF. URL <https://www.science.org/doi/10.1126/sciadv.1501495>.
- E. Saucan, A. Samal, and J. Jost. A Simple Differential Geometry for Complex Networks. *Network Science*, 9(S1):S106–S133, 4 2020. ISSN 20501250. doi: 10.48550/arxiv.2004.11112. URL <https://arxiv.org/abs/2004.11112v2>.
- I. J. Schoenberg. Remarks to Maurice Frechet’s Article “Sur La Definition Axiomatique D’Une Classe D’Espace Distances Vectoriellement Applicable Sur L’Espace De Hilbert. *The Annals of Mathematics*, 36(3):724, 7 1935. ISSN 0003486X. doi: 10.2307/1968654.
- J. Sia, E. Jonckheere, and P. Bogdan. Ollivier-Ricci Curvature-Based Method to Community Detection in Complex Networks. *Nature, Scientific Reports 2019 9:1*, 9(1):1–12, 7 2019. ISSN 2045-2322. doi: 10.1038/s41598-019-46079-x. URL <https://www.nature.com/articles/s41598-019-46079-x>.

- A. Sklar. Fonctions de repartition a n dimensions et leurs marges. *Publications de l'Institut de statistique de l'Université de Paris*, 8:229–231, 1959. URL <https://ci.nii.ac.jp/naid/10011938360>.
- A. L. Smith, D. M. Asta, and C. A. Calder. The Geometry of Continuous Latent Space Models for Network Data. *Statistical Science*, 34(3):428–453, 12 2017. ISSN 21688745. doi: 10.48550/arxiv.1712.08641. URL <https://arxiv.org/abs/1712.08641v2>.
- T. Sweet and S. Adhikari. A Latent Space Network Model for Social Influence. *Psychometrika*, 85(2):251–274, 6 2020. ISSN 18600980. doi: 10.1007/S11336-020-09700-X/FIGURES/11. URL <https://link.springer.com/article/10.1007/s11336-020-09700-x>.
- P. van der Hoorn, W. J. Cunningham, G. Lippner, C. Trugenberg, and D. Krioukov. Ollivier-Ricci curvature convergence in random geometric graphs. *Physical Review Research*, 3(1), 8 2020. doi: 10.1103/PhysRevResearch.3.013211. URL <http://arxiv.org/abs/2008.01209><http://dx.doi.org/10.1103/PhysRevResearch.3.013211>.
- A. van der Vaart. *Asymptotic Statistics*. Cambridge University Press, 10 1998. doi: 10.1017/cbo9780511802256. URL </core/books/asymptotic-statistics/A3C7DAD3F7E66A1FA60E9C8FE132EE1D>.
- E. M. Volz, J. C. Miller, A. Galvani, and L. Meyers. Effects of Heterogeneous and Clustered Contact Patterns on Infectious Disease Dynamics. *PLOS Computational Biology*, 7(6):e1002042, 2011. ISSN 1553-7358. doi: 10.1371/JOURNAL.PCBI.1002042. URL <https://journals.plos.org/ploscompbiol/article?id=10.1371/journal.pcbi.1002042>.
- S. Zhang, Y. Tay, W. Jiang, D.-c. Juan, and C. Zhang. Switch spaces: learning product spaces with sparse gating. *arXiv preprint arXiv:2102.08688*, 2021.

A Proofs of Theorems

A.1 Proof of Lemma 1

Proof. Consider first a set of 3 points on $(x, y, z) \in \mathbb{S}^p$ which are not co-linear. We can define an orthogonal matrix (rotation matrix) $Q \in \mathbb{R}^{p+1 \times p+1}$ which we will first construct a rotational isometry, then use a result which exploits fixed point isometries.

Theorem 11 (Theorem 1.10.15 in Klingenberg [1995]). *If $f : (\overline{M}, \overline{g}) \rightarrow (\overline{M}, \overline{g})$ is an isometry on a Riemannian manifold, then the fixed point set of f forms a totally geodesic submanifold.*

WLOG let $x = (1, 0, \dots, 0)$. We define the orthogonal rotation matrix Q via the following. Let q_i denote the i^{th} un-normalized column vector of Q . We the define the

following first 3 basis functions

$$\begin{aligned} q_1 &= [1, 0, \dots, 0]^\top \\ q_2 &= y - (y^\top q_1)q_1 \\ q_3 &= z - \frac{(z^\top q_2)}{\|q_2\|_2}q_2 - (z^\top q_1)q_1 \end{aligned}$$

Then normalizing each of these vectors to construct the columns of Q and completing the orthonormal basis with any remaining orthogonal basis vectors of \mathbb{R}^p , and we have constructed an orthogonal matrix Q and $Q^\top Q = I = QQ^\top$. Thus we have defined an isomorphism $f_1(\cdot) : \mathbb{S}^p \mapsto \mathbb{S}^p$ where

$$\begin{aligned} f_1(x) &= Q^\top x \\ d(f_1(x), f_1(y)) &= \frac{1}{\sqrt{\kappa}} \operatorname{acos} \left(f_1(x)^\top f_1(y) \right) \\ &= \frac{1}{\sqrt{\kappa}} \operatorname{acos} \left(x^\top QQ^\top y \right) \\ &= \frac{1}{\sqrt{\kappa}} \operatorname{acos} \left(x^\top y \right) \\ &= d(f_1(x), f_1(y)) \end{aligned}$$

hence this rotation is an isomorphism. Then let $f_2(x) = (x_0, x_1, x_2, -x_3, -x_4, \dots, -x_p)$ denote an additional isomorphism. Since the composition of isomorphisms is also an isomorphism, we can define a totally geodesic submanifold of dimension 2 which consists of the solution set to $Q^\top = [c_1, c_2, c_3, 0, 0, \dots, 0]^\top$ for some c_1, c_2, c_3 by Theorem 11. Then clearly, x, y, z are all fixed points of this isomorphism by construction, and hence any three points can be contained within a totally geodesic submanifold of dimension 2 of the corresponding curvature.

The proofs for \mathbb{E}^p and \mathbb{H}^p follows this argument identically and thus the proof is complete. \square

A.2 Proof of Theorem 2

Proof. Any 3 points (x, y, z) can be embedded isometrically in a totally geodesic submanifold of dimension 2 when $\mathcal{M}^p(\kappa)$ is a canonical manifold due to Lemma 1.

Case 1: Spherical. Under the spherical model, first place the midpoint at the origin. Next, given d_{yz} place point y at the point $(y_0, y_1, 0)$ where $y_1 = \sqrt{1 - y_0^2}$. Then $y_0 = \cos(\sqrt{\kappa} \frac{d_{yz}}{2})$. Next we place point z at $z = (z_0, z_1, 0)$ where $z_0 = y_0$ and $z_1 = -y_1$. Third, we solve for the locations of x such that d_{xm}, d_{xy}, d_{xz} are satisfied.

We continue with $x = (x_0, x_1, x_2)$. We can set $x_0 = \cos(\sqrt{\kappa} \frac{d_{xm}}{2})$. Next, x_1 can be solved by letting

$$\begin{aligned} \cos(\sqrt{\kappa} d_{xy}) &= x_0 y_0 + x_1 y_1 \\ &= \cos(\sqrt{\kappa} d_{xm}) \cos(\sqrt{\kappa} d_{yz}/2) + x_1 \sin(\sqrt{\kappa} d_{yz}/2) \end{aligned}$$

Similarly

$$\begin{aligned} \cos(\sqrt{\kappa} d_{xz}) &= x_0 z_0 + x_1 z_1 \\ &= \cos(\sqrt{\kappa} d_{xm}) \cos(\sqrt{\kappa} d_{yz}/2) - x_1 \sin(\sqrt{\kappa} d_{yz}/2) \end{aligned}$$

solving for x_1 results in:

$$\frac{\cos(\sqrt{\kappa}d_{xy}) - \cos(\sqrt{\kappa}d_{xm}) \cos(\sqrt{\kappa}d_{yz}/2)}{\cos(\sqrt{\kappa}d_{xz}) - \cos(\sqrt{\kappa}d_{xm}) \cos(\sqrt{\kappa}d_{yz}/2)} = -1$$

which can be further rearranged to

$$2 \cos(d_{xm}\sqrt{\kappa}) - \text{Sec}\left(\frac{d_{yz}}{2}\sqrt{\kappa}\right)(\cos(d_{xy}\sqrt{\kappa}) + \cos(d_{xz}\sqrt{\kappa})) = 0$$

We then normalize this by the curvature value $\frac{1}{\kappa}$, which allows for $g(\kappa, d)$ to be a continuous function of κ from the hyperbolic $\kappa < 0$ to spherical space $\kappa > 0$.

Case 2: Hyperbolic. The proof of the hyperbolic case follows an identical method to the spherical case and is omitted for brevity. However this results in the estimating function:

$$\begin{aligned} & \frac{1}{-\kappa} \left(2 \cosh(d_{xm}\sqrt{-\kappa}) \right. \\ & \left. - \text{Sech}\left(\frac{d_{yz}}{2}\sqrt{-\kappa}\right)(\cosh(d_{xy}\sqrt{-\kappa}) + \cosh(d_{xz}\sqrt{-\kappa})) \right) = 0 \end{aligned}$$

Remark: Under the limit as $\kappa \rightarrow 0$ we find that $\lim_{\kappa \rightarrow 0} g(\kappa, d) = \frac{1}{2}d_{xy}^2 + \frac{1}{2}d_{xz}^2 - \frac{1}{4}d_{yz}^2 - d_{xm}^2$ which gives exactly the parallelogram law in Euclidean space. This also highlights the necessity that the term $\frac{1}{\kappa}$ plays in maintaining a smooth equation as a function of κ through 0. \square

A.3 Proof of Theorem 3

Proof. We will use the implicit function theorem to construct an implicit function for which we can later apply a delta method. We first note that $g(\kappa, d)$ is continuously differentiable when $\sqrt{\kappa} < \frac{\text{acos}(\pi)}{d_{yz}}$. This boundary, however corresponds to the maximum distance allowed on a sphere, as given by two anti-polar points. Therefore to apply the implicit function theorem, what remains is

$$\frac{\partial}{\partial \kappa} g(\kappa, d) \neq 0.$$

which will hold by a brief application of (B3). As we have derived in Theorem2, $d_{xm}(\kappa; \mathbf{d}(x, y, z))$ is a differentiable, continuous function.

We note that since by definition, the function

$$g(\kappa, d_{xy}, d_{xz}, d_{yz}, d_{xm}(\kappa; \mathbf{d}(x, y, z))) = 0$$

Therefore, it is equivalent for a fixed d_{xm} to write the estimating function as a function of the equivalent exact midpoint $d_{xm}(\kappa)$ ¹

$$g(\kappa; d_{xy}, d_{xz}, d_{yz}, d_{xm}) = \frac{2 \cos(d_{xm}\sqrt{\kappa})}{\kappa} - \frac{2 \cos(d_{xm}(\kappa)\sqrt{\kappa})}{\kappa}$$

Computing the derivative as a function of κ

¹We drop the $\mathbf{d}(x, y, z)$ for brevity

$$\begin{aligned}
& \left. \frac{d}{d\kappa'} g(\kappa'; d_{xy}, d_{xz}, d_{yz}, d_{xm}) \right|_{\kappa'=\kappa} \\
&= 2 \frac{-d_{xm} \sqrt{\kappa} \sin(d_{xm} \sqrt{\kappa}) + 2 \cos(d_{xm} \sqrt{\kappa})}{2\kappa^2} \\
&+ 2 \frac{(d_{xm}(\kappa) \sqrt{\kappa} + \kappa^{3/2} d'_{xm}(\kappa)) \sin(d_{xm} \sqrt{\kappa}) - 2 \cos(d_{xm}(\kappa) \sqrt{\kappa})}{2\kappa^2}
\end{aligned}$$

Since $g(\kappa, \mathbf{d}) = 0 \implies d_{xm} = d_{xm}(\kappa)$,

$$\left. \frac{d}{d\kappa'} g(\kappa'; d_{xy}, d_{xz}, d_{yz}, d_{xm}) \right|_{\kappa'=\kappa} = 2d'_{xm}(\kappa) \frac{\sin(d_{xm}(\kappa) \sqrt{\kappa})}{\sqrt{\kappa}}$$

Since $\kappa \leq \frac{\pi^2}{d_{xm}^2}$ then if $d'_{xm}(\kappa) > 0$ then $\frac{d}{d\kappa} g(\kappa, \mathbf{d}) > 0$

Next, by the implicit function theorem, there exists an open neighborhood $\mathcal{D} \in \mathbb{R}^4$ and a function $f(d)$ such that $\kappa = f(d)$ and $g(f(d), d)$. Furthermore:

$$\nabla_d f(d) = - \left(\frac{\partial g(\kappa, d)}{\partial \kappa} \right)^{-1} [\nabla_d g(\kappa, d)]$$

Therefore by the delta method:

$$\begin{aligned}
\sqrt{r(n)}(\hat{\kappa} - \kappa) &= \sqrt{r(n)}(f(\hat{d}) - f(d)) \\
&\rightarrow_W N(0, \nabla g(d)^\top \Sigma \nabla g(d))
\end{aligned}$$

And by the implicit function theorem:

$$\nabla g(d)^\top \Sigma \nabla g(d) = \left(\frac{\partial g(\kappa, d)}{\partial \kappa} \right)^{-1} \left[\nabla_d g(\kappa, d)^\top \Sigma \nabla_d g(\kappa, d) \right]$$

If instead $\|\hat{d} - d\|_2 = o_P(r(n)^{-1/2})$, then we can use the continuous mapping theorem instead and we have $|\hat{\kappa} - \kappa| = o_P(r(n)^{-1/2})$. **Remark:** This form is very similar to the usual standard asymptotic normality proofs for Z estimators as in van der Vaart [1998]. However, the main difference is in the fact that we are not averaging the estimating function, but rather plugging in a distance estimate which is asymptotically normal.

We find that in practice, condition (B3) holds, however, for some distances that are plugged in, particularly those which may not satisfy a midpoint exactly may result in the root of the estimating function be the root of its partial derivative. In fact, in the Euclidean case, according to the Taylor series expansion at $\kappa = 0$

$$\begin{aligned}
g(\kappa; d) &= \left(\frac{d_{xy}^2}{2} + \frac{d_{xz}^2}{2} - d_{xm}^2 - \frac{d_{yz}^2}{4} \right) + \\
&\left(\frac{d_{xm}^2}{12} - \frac{5d_{yz}^2}{192} + \frac{1}{16} d_{yz}^2 (d_{xy}^2 + d_{xz}^2) - \frac{1}{24} (d_{xy}^2 + d_{xz}^2) \right) \kappa \\
&+ \mathcal{O}(\kappa^2).
\end{aligned}$$

Clearly at $\kappa = 0$ the solution reduces to the parallelogram law ($\frac{d_{xy}^2}{2} + \frac{d_{xz}^2}{2} - d_{xm}^2 - \frac{d_{yz}^2}{4} = 0$). When we substitute in the corresponding solution at $\kappa = 0$.

$$\begin{aligned} \left. \frac{\partial}{\partial \kappa} g(\kappa; d) \right|_{\kappa=0} &= -\frac{1}{48} (d_{yz}^4 - 2d_{yz}^2(d_{xz}^2 + (d_{xy}^2) + (d_{xz}^2 - d_{xy}^2)^2) \\ &= -\frac{1}{48} \left((d_{yz} + d_{xz} + d_{xy})(d_{yz} - d_{xz} - d_{xy}) \right. \\ &\quad \left. \times (d_{yz} - d_{xz} + d_{xy})(d_{yz} + d_{xz} - d_{xy}) \right) \end{aligned}$$

As long as the triangle inequality is satisfied strictly for x, y, z , then $\left. \frac{\partial}{\partial \kappa} g(\kappa; d) \right|_{\kappa=0} > 0$. However, if the triangle inequality is not strict, i.e. x, y, z are co-linear, and $d_{ij} = d_{ik} + d_{kj}$ for (i, j, k) being some permutation of (x, y, z) , then $\left. \frac{\partial}{\partial \kappa} g(\kappa; d) \right|_{\kappa=0} = 0$.

For $\kappa \neq 0$, we do not have simple closed-form expressions for $\left. \frac{\partial}{\partial \kappa} g(\kappa; d) \right|_{\kappa=0}$ and thus we leave (B3) as an assumption, however, we believe this trend to hold in the other canonical manifolds. □

Lemma 12. *Let $x, y, z \in \mathcal{M}^P(\kappa)$ and let m denote the midpoint between y and z . Then let $d_{xm}(\kappa; \mathbf{d}(x, y, z))$ denote the distance to the midpoint m from x as a function of the curvature of the latent space κ .*

Then $d_{xm}(\kappa; \mathbf{d}(x, y, z))$ is an increasing function in κ .

Proof. The proof follows from Toponogov's triangle theorem and the negative curvature extension [Berger, 1962]. Abbreviated for our purposes in Theorem 13, we simply let $p = z, x = r, q = m$ and compare two manifolds $\kappa \leq \kappa'$.

Then it immediately follows

$$d_{xm}(\kappa; \mathbf{d}(x, y, z)) \leq d_{xm}(\kappa'; \mathbf{d}(x, y, z)).$$

□

Theorem 13 (Toponogov's Triangle Comparison Theorem (Theorem 3 of Berger [1962])). *Let \mathcal{M} be a complete Riemannian manifold, and let (κ) be the simply connected manifold of constant curvature $\kappa \in \mathbb{R}$. Let Δ_{pqr} denote a geodesic triangle with points $p, q, r \in \mathcal{M}$. Let $\tilde{\Delta}_{pqr}$ is the geodesic triangle with side lengths $d_{pq} = \tilde{d}_{pq}$ and $d_{pr} = \tilde{d}_{pr}$. If $\underline{K}(\mathcal{M})$ is the minimum Riemannian sectional curvature on the manifold, and if $\kappa \leq \underline{K}(\mathcal{M})$, then*

$$\tilde{d}_{qr} \leq d_{qr}.$$

Assumption (B3) is therefore very mild and that we will always have a non-decreasing d_{xm} function of κ but that we only have to assume that the increasingness is strict. In practice, this is only not strict when the points x, y, z are colinear, and therefore the distance to the midpoint does not change as a function of the curvature since, effectively, these points lie along a single geodesic.

A.4 Proof of Theorem 10

Proof. The proof here is a straightforward application of the plug in estimator of \hat{p}_{XY} and the set of random effects $\hat{\gamma}_{X/Y}$. Then by the Lindeberg-Feller CLT:

$$\sqrt{\ell^2 \sigma_\ell} (\hat{p}_{XY} - p_{XY}) \rightarrow_d N(0, 1)$$

Plugging this in to our definition of distance

$$\begin{aligned} \hat{d}_{XY} &= -\log(\hat{p}_{XY}) + \hat{\gamma}_X + \hat{\gamma}_Y \\ \sqrt{\ell^2} \hat{d}_{XY} &= -\sqrt{\ell^2} \log(\hat{p}_{XY}) + \sqrt{\ell^2} \hat{\gamma}_X + \sqrt{\ell^2} \hat{\gamma}_Y \\ &= -\sqrt{\ell^2} \log(\hat{p}_{XY}) + o_P(1) \end{aligned}$$

And by the delta method:

$$\sqrt{\ell^2 \frac{\sigma_\ell}{p_{XY}}} (\hat{d}_{XY} - d_{XY}) \rightarrow_d N(0, 1)$$

□

A.5 Proof of Theorem 5

In order to prove Theorem 5 we first prove a series of lemmas.

Let F denote a marginal distribution (in our case that of $\Xi(m)$) and let X_i be a random variable with distribution function F . By Sklar's Theorem [Sklar, 1959, Durante et al., 2013] we can express the joint distribution (H) of a vector of correlated X, H as

$$\begin{aligned} H(\mathbf{x}) &= P(X_1 \leq x_1, X_2 \leq x_2, \dots, X_n \leq x_n) \\ &= \mathbb{C}(F(x_1), F(x_2), \dots, F(x_n)) \end{aligned}$$

where \mathbb{C} is a copula for the joint distribution.

Lemma 14. *For a set of random variables X_i with equal marginal distribution, with arbitrary correlation structure denoted via copula \mathbb{C} , then $\hat{\mathbb{M}}(X) = F^{-1}(\hat{\mathbb{M}}(U))$ where $U \sim \mathbb{C}$*

Proof. We can express $X = F^{-1}(U)$ where U is sampled from the copula \mathbb{C} . Then if n is odd, $X_{((n+1)/2)}$ is the median, and clearly $X_{(i)} = F^{-1}(U_{(i)})$ with the subscript (i) denoting the i^{th} order statistic. Now consider n which is even. If z is a median of U then $z \in [U_{(n/2)}, U_{(n/2+1)}]$ then

$$\begin{aligned} z &\in [U_{(n/2)}, U_{(n/2+1)}] \\ \iff F^{-1}(z) &\in [F^{-1}(U_{(n/2)}), F^{-1}(U_{(n/2+1)})] \\ \iff F^{-1}(z) &\in [X_{(n/2)}, X_{(n/2+1)}] \end{aligned}$$

Hence medians of X . Hence medians of the underlying uniform distribution are mapped to the median of the observed variables. □

This lemma suggests that if we take the median of the underlying generative uniforms of the set of correlated random variables.

Lemma 15. Consider a set $A_I = \cap_{i \in I} \{U_i \leq z\}$ where I is a subset of $\{1, 2, \dots, n\}$. Consider a sequence of sets A_j such that any pair of j, j' contain at least 1 overlapping index. Then

$$\mathbb{C}(\cup A_j) \leq \mathbb{W}(\cup A_j) \quad (17)$$

where \mathbb{W} is the perfectly collinear measure corresponding to the upper Fréchet Hoeffding Bound [Frechet, 1957, Hoeffding, 1940].

Proof. We prove this by induction. Consider the base case A_1, A_2 . Suppose there exists some copula \mathbb{Q} such that $\mathbb{Q}(A_1 \cup A_2) > \mathbb{W}(A_1 \cup A_2)$. Firstly under \mathbb{W}

$$\begin{aligned} \mathbb{W}(A_1 \cup A_2) &= \mathbb{W}(A_1) + \mathbb{W}(A_2) - \mathbb{W}(A_1 \cap A_2) \\ &= \min\{1, z\} + \min\{1, z\} - \min\{1, z\} \\ &= z + z - z \\ &= z \end{aligned}$$

Then since $\{A_j, \cup A_{j'}\} \subset \{U_k \leq z\}$ for some index k . Then

$$\mathbb{Q}(A_1 \cup A_2) \leq \mathbb{Q}(U_k \leq z)$$

However, then $\mathbb{Q}(U_k \leq z) > z$ and thus \mathbb{Q} is not a copula. Now suppose the following holds for any \mathbb{Q} .

$$\mathbb{Q}(\cup_{j=1}^n A_j) \leq \mathbb{W}(\cup_{j=1}^n A_j)$$

for some n . Denote $B = \cup_{j=1}^n A_j$ then we show:

$$\mathbb{Q}(B \cup A_{n+1}) \leq \mathbb{W}(B \cup A_{n+1})$$

Suppose that there exists \mathbb{Q} such that $\mathbb{Q}(B \cup A_{n+1}) > \mathbb{W}(B \cup A_{n+1})$

$$\mathbb{W}(B \cup A_{n+1}) = \mathbb{W}(B) + \mathbb{W}(A_{n+1}) - \mathbb{W}(B \cap A_{n+1})$$

Clearly, $\mathbb{W}(B) = z$, $\mathbb{W}(A_{n+1}) = z$ and $\mathbb{W}(B \cap A_{n+1}) = z$. Then $\mathbb{Q}(B \cup A_{n+1}) = \mathbb{Q}(B) + \mathbb{Q}(A_{n+1}) - \mathbb{Q}(B \cap A_{n+1})$. Therefore

$$\mathbb{Q}(B \cup A_{n+1}) \leq z + \underbrace{\mathbb{Q}(A_{n+1}) - \mathbb{Q}(B \cap A_{n+1})}_{\geq 0}$$

which generates a contradiction hence

$$\mathbb{Q}(B \cup A_{n+1}) \leq \mathbb{W}(B \cup A_{n+1})$$

□

Lemma 16. For any copula, \mathbb{C}

$$\mathbb{C}(\widehat{\mathbb{M}}(U) \leq z) \leq 2z \quad (18)$$

Proof. Define the events A_j as in Lemma 15 of size $\lceil n/2 \rceil$. Then the event $\{\widehat{\mathbb{M}}(U) \leq z\}$ is equal to the union of all such A_j as the median will be equivalent to the case when at least half of all uniforms are below z . We can partition A_j into two sets S_1, S_2 for which any two pairs of A_j in a set have at least one overlapping index. This can be done by taking all the sets A_j containing $\{U_1 \leq z\}$ in their index and placing them into set S_1 . Then all other sets must be placed in set S_2 . Since there are $(n - 1)$ possible remaining indices $\{2, 3, \dots, n\}$ available for S_2 then any two events must have an overlapping index (by the pigeonhole principle). Therefore

$$\begin{aligned} \mathbb{C}(\widehat{\mathbb{M}}(U) \leq z) &= \mathbb{C}(\cup A_i) \\ &= \mathbb{C}(S_1 \cup S_2) \\ &\leq \mathbb{C}(S_1) + \mathbb{C}(S_2) \text{ Union Bound} \\ &\leq \mathbb{W}(S_1) + \mathbb{W}(S_2) \text{ Lemma 15} \\ &= 2z \end{aligned}$$

□

For our theorem, this is all we need, but a corollary immediately follows. This relates the concentration of any set of arbitrarily correlated uniforms to the concentration of a singular component element.

Corollary 17. *For any copula \mathbb{C} .*

$$\mathbb{C}(|\widehat{\mathbb{M}}(U) - 1/2| > \epsilon) \leq 2P(|U - 1/2| > \epsilon) \quad (19)$$

Proof. $P(|U - 1/2| > \epsilon)$ is simply the marginal distribution of a uniform distribution.

$$P(|U - 1/2| > \epsilon) = \max\{1 - 2\epsilon, 0\}$$

Next we note that

$$\{|\widehat{\mathbb{M}}(U) - 1/2| > \epsilon\} = \{\widehat{\mathbb{M}}(U) < 1/2 - \epsilon\} \cap \{\widehat{\mathbb{M}}(U) > 1/2 + \epsilon\}$$

Note that we can define $1 - V = U$ where the measure of V , $\widetilde{\mathbb{C}}$ is also a copula, since this is a joint distribution of marginally uniform variables.

$$\{\widehat{\mathbb{M}}(U) > 1/2 + \epsilon\} = \{\widehat{\mathbb{M}}(V) < 1/2 - \epsilon\}$$

hence by a union bound.

$$\begin{aligned} \mathbb{C}(|\widehat{\mathbb{M}}(U) - 1/2| > \epsilon) &\leq \mathbb{C}(\widehat{\mathbb{M}}(U) < 1/2 - \epsilon) + \widetilde{\mathbb{C}}(\widehat{\mathbb{M}}(V) < 1/2 - \epsilon) \\ &= 2(1/2 - \epsilon) + 2(1/2 - \epsilon) \end{aligned}$$

then since the copula is non-negative

$$\begin{aligned} \mathbb{C}(|\widehat{\mathbb{M}}(U) - 1/2| > \epsilon) &\leq 2 \max\{1 - 2\epsilon, 0\} \\ &= 2P(|U - 1/2| > \epsilon) \end{aligned}$$

□

Lemma 18. *For any set of marginally identically distributed random variables $\{X_i\}_{i=1}^n$ with CDF F generated with an arbitrary copula \mathbb{C} , then:*

$$P(\widehat{\mathbb{M}}(X) \leq t) \leq 2P(X_1 \leq t) \quad (20)$$

Proof. The proof immediately is a result of Lemma 14 and 16.

$$\begin{aligned} P(\widehat{\mathbb{M}}(X) \leq t) &= \mathbb{C}(F^{-1}(\widehat{\mathbb{U}}) \leq t) \text{ Lemma 14} \\ &= \mathbb{C}(\widehat{\mathbb{U}} \leq F(t)) \\ &\leq 2P(U \leq F(t)) \text{ Lemma 16} \\ &= 2F(t) \\ &= 2P(X_1 \leq t) \end{aligned}$$

□

This concludes the proof of Theorem 5

A.6 Proof of Theorem 4

Proof. Denote the set of events $M_i(t) = \widehat{\mathbb{M}}[\Xi(Z_{\{1, \dots, i\}})] > t$ and let $G = \cap_{i=1}^K M_i(t)$. We can upper bound the probability that $\Phi(\mathcal{D}_K) \leq t$ by the following:

$$\begin{aligned} &P(\Phi(\mathcal{D}_K) \leq t) \\ &= P(\Phi(\mathcal{D}_K) \leq t | \Phi(\mathcal{D}_{K-1}) \leq t, G)P(\Phi(\mathcal{D}_{K-1}) \leq t | G)P(G) \\ &+ P(\Phi(\mathcal{D}_K) \leq t | \Phi(\mathcal{D}_{K-1}) > t, G)P(\Phi(\mathcal{D}_{K-1}) > t | G)P(G) \\ &+ P(\Phi(\mathcal{D}_K) \leq t | G^c)P(G^c) \\ &\leq \underbrace{P(\Phi(\mathcal{D}_K) \leq t | \Phi(\mathcal{D}_{K-1}) \leq t, G)}_{(I)}P(\Phi(\mathcal{D}_{K-1}) \leq t | G) + \underbrace{P(G^c)}_{(II)} \end{aligned}$$

We first consider (I). Since we assume G at each step, at least half of the midpoints are at a distance t away. Therefore:

$$\begin{aligned} (I) &= P(\Phi(\mathcal{D}_K) \leq t | \Phi(\mathcal{D}_{K-1}) \leq t, G) \\ &\leq \max\{0, 1 - \binom{K}{2} \alpha \frac{C_p}{2} t^p\} \\ &\leq \exp\left(-\binom{K}{2} \alpha \frac{C_p}{2} t^p\right) \end{aligned}$$

By recursion, we can apply this such that:

$$\begin{aligned} \prod_{k=1}^K P(\Phi(\mathcal{D}_K) \leq t | \Phi(\mathcal{D}_{K-1}) > t, G) &\leq \exp\left(-\sum_{k=1}^K \binom{k}{2} \alpha \frac{C_p}{2} t^p\right) \\ &= \exp\left(-\binom{K+1}{3} \alpha \frac{C_p}{2} t^p\right) \\ &\leq \exp\left(-(K+1)^3 \alpha \frac{C_p}{12} t^p\right) \end{aligned}$$

Secondly let we consider term (II). Then

$$\begin{aligned}
P(G^c) &= P(\cup_{k=1}^K \{\widehat{\mathbb{M}}[\Xi(Z_{\{1,\dots,k\}})] \leq t\}) \\
&\leq \sum_{k=1}^K P(\widehat{\mathbb{M}}[\Xi(Z_{\{1,\dots,k\}})] \leq t) \\
&\leq K(P(\widehat{\mathbb{M}}[\Xi(Z_K)] \leq t))
\end{aligned}$$

Since by definition, the median distance to the closest midpoint will be decreasing as we add more points. Next, by Lemma 16

$$\begin{aligned}
P(\{\widehat{\mathbb{M}}[\Xi(Z_K)] \leq t\}) &\leq 2P(\Xi(Z_K) \leq t) \\
&= 2P(\cup_{m' \neq m} d(m, m') \leq t) \\
&\leq 2 \sum_{m' \neq m} P(d(m, m') \leq t)
\end{aligned}$$

And by assumption in our theorem $P(d(m, m') \leq t) \leq C_p t^p$. Hence we combine these bounds

$$P(\Phi(\mathcal{D}_K) \leq t) \leq \exp(-(K+1)^3 \alpha \frac{C_p}{12} t^p) + 2K \binom{K}{2} t^p$$

Letting $t = \frac{C_2}{K^{3/q}}$ will allow bounding $P(\Phi(\mathcal{D}_K) \leq t)$ by any constant and therefore:

$$\Phi(\mathcal{D}_K) = \mathcal{O}_P(K^{-3/q})$$

□

A.7 Proof of Theorem 6

Proof. The proof is straightforward, let $\mathbf{d}(x, y, z)$ denote the vector of the distances of the triangle (x, y, z) , and let $\mathbf{d}(m', y, z)$ be the distances in the triangle (m', y, z) . Suppose also that we have the distance $d_{xm'}$ as this is the distance to the surrogate point, used as a midpoint. Though we do not have access to the true distance d_{xm} , this is a function of the curvature, and can be written as $d_{xm}(\kappa; \mathbf{d}(x, y, z))$. If we assume that we have a point m' , so that $m', x, y, z, \in \mathcal{M}^p(\kappa)$, then we can also define $d_{m'm}(\kappa; \mathbf{d}(m', y, z))$. By the triangle inequality,

$$\begin{aligned}
d_{xm}(\kappa; \mathbf{d}(x, y, z)) &\leq d_{xm'} + d_{m'm}(\kappa; \mathbf{d}(m', y, z)) \\
d_{xm}(\kappa; \mathbf{d}(x, y, z)) &\geq d_{xm'} - d_{m'm}(\kappa; \mathbf{d}(m', y, z))
\end{aligned}$$

By Lemma 12 each d_{xm} function is monotone in κ . Therefore, the number of solutions in κ can either be $\{0, 1, \infty\}$. If d_{xm} never intersect, then it is 0, if they intersect once, then it is 1, or if they remain equal for a region of κ then it is ∞ . This can be rearranged so that these solutions satisfy.

$$\begin{aligned}
g(\kappa, \mathbf{d}(x, y, z), d_{xm'} + d_{m'm}(\kappa; \mathbf{d}(m', y, z))) &= 0 \\
g(\kappa, \mathbf{d}(x, y, z), d_{xm'} - d_{m'm}(\kappa; \mathbf{d}(m', y, z))) &= 0
\end{aligned}$$

If there is a single solution, then this becomes a single upper or lower bound. If there are no solutions, then the upper and lower bounds are $\pm\infty$, and if there are infinite solutions, we may take the most conservative of these. □

A.8 Proof of Lemma 7

The proof draws on a similar structure to that of the consistency result of Lubold et al. [2023], though we highlight the convergence rate achieved under mild assumptions.

Proof. Let $\epsilon_\delta := \{\delta < \delta\}$. We wish to show that:

$$\lim_{\ell \rightarrow \infty} \frac{P(\epsilon_\delta | C_\ell)}{P(\epsilon_\delta^c | C_\ell)} \rightarrow \infty$$

for $\delta = O(\exp(-\ell))$.

$$\begin{aligned} P(C_\ell | \epsilon_\delta) &= \int \int_{\epsilon_\delta} \exp\left(-\binom{\ell}{2} \bar{d}(z)\right) \exp\left(-\binom{\ell}{2} \bar{\nu}\right) dP_{Z|\epsilon_\delta}(z) dP_\nu(\nu) \\ &= \Psi(P_\nu) \int_{\epsilon_\delta} \exp\left(-\binom{\ell}{2} \bar{d}(z)\right) dP_{Z|\epsilon_\delta}(z) \\ \text{where } \Psi(P_\nu) &= \int \exp\left(-\binom{\ell}{2} \bar{\nu}\right) dP_\nu(\nu). \end{aligned}$$

This can be developed analogously for $P(C_\ell | \epsilon_\delta^c)$ allowing us to ignore the random effects in this analysis.

Next, consider the ball of radius $\frac{\delta}{2}$ at a point $q \in B(\delta, q)$. This describes one set of points for which all points have a maximal distance of δ . Then $\{Z_i\}_{i=1}^\ell \in B(\delta, q) \implies \epsilon_\delta$ for any q . Since f is continuous, then for some $\tilde{\delta}$ if $f(q)$ has positive probability $f(q) > 0$ for some q then for all $\delta \leq \tilde{\delta}$, $f(x) \geq c_2; \forall x \in B(q, \delta)$ for some constant c . Therefore $P(\epsilon_\delta) \geq P(\{Z_i\}_{i=1}^\ell \in B(\delta, q)) \geq \left(c_2 \left(\frac{\delta}{2}\right)^p\right)^\ell$.

Furthermore from Lemma A.1 in Lubold et al. [2023]

$$P(C_\ell | \epsilon_\delta^c) \leq \exp\left(-\binom{\ell}{2} \mu_d\right)$$

Putting this all together, for $P(\epsilon_\delta) \leq \frac{1}{2}$

$$\begin{aligned} \frac{P(\epsilon_\delta | C_\ell)}{P(\epsilon_\delta^c | C_\ell)} &= \frac{P(C_\ell | \epsilon_\delta)}{P(C_\ell | \epsilon_\delta^c)} \frac{P(\epsilon_\delta)}{1 - P(\epsilon_\delta)} \\ &\geq \frac{P(C_\ell | \epsilon_\delta)}{P(C_\ell | \epsilon_\delta^c)} \frac{1}{2} P(\epsilon_\delta) \\ &\geq \frac{1}{2} \frac{P(C_\ell | \epsilon_\delta)}{P(C_\ell | \epsilon_\delta^c)} c_2^\ell \left(\frac{\delta}{2}\right)^{p\ell} \\ &\geq \frac{1}{2} \frac{\exp\left(-\binom{\ell}{2} \delta\right)}{P(C_\ell | \epsilon_\delta^c)} c_2^\ell \left(\frac{\delta}{2}\right)^{p\ell} \\ &\geq \frac{1}{2} \frac{\exp\left(-\binom{\ell}{2} \delta\right)}{\exp\left(-\binom{\ell}{2} \mu_d\right)} c_2^\ell \left(\frac{\delta}{2}\right)^{p\ell} \\ &= \frac{1}{2} \exp\left(-\binom{\ell}{2} \delta + \binom{\ell}{2} \mu_d + \ell \log(c_2) + \log(\delta/2) p\ell\right) \end{aligned}$$

Therefore letting $\delta = 2 \exp(-\tilde{\mu}_d \frac{\ell-1}{p})$ for $\tilde{\mu}_d < \mu_d$. Then

$$\lim_{\ell \rightarrow \infty} \frac{P(\epsilon_\delta | C_\ell)}{P(\epsilon_\delta^c | C_\ell)} \rightarrow \infty$$

and therefore the proof is complete. \square

A.9 Proof of Lemma 8

At a high level, the proof structure is nearly identical to Lemma 7, however, we swap the roles of ν and $d(Z_i, Z_j)$.

Proof. Let $\epsilon_\delta = \{\min_{i \in \{1, 2, \dots, \ell\}} \nu_i \geq -\delta\}$

If $f_\nu(\nu)$ is smooth and has left side derivative around 0 then for small enough δ , $F_\nu(\nu > -\delta) \geq c_3 \delta$. As in the previous method, we similarly take the ratio and integrate out $\Psi(P_{\vec{d}})$.

Then consider the set $[-\delta, 0]$. Then $P(\epsilon_\delta) \geq (c_3(\delta))^\ell$.

Next we consider the probability of a clique, conditional on the fact that the locations did not occur in set ϵ_δ^c .

$$P(C_\ell | \epsilon_\delta^c) \leq \int \exp\left(2 \binom{\ell}{2} \bar{\nu}\right) dP_\nu(\nu)$$

where $\nu d = \frac{1}{\ell} \sum_{i < j} \nu$ Let $\mu_\nu = \mathbb{E}[\nu]$. This is due to the fact ϵ_δ denotes the event that $\min_i \nu < -\delta$ it is reasonable that $P(C_\ell | \epsilon_\delta^c) \geq P(C_\ell)$ since we are excluding the events most likely to create a clique. Furthermore by the same argument as in Lemma A.1 in Lubold et al. [2023]

$$P(C_\ell | \epsilon_\delta^c) \leq \exp(2 \binom{\ell}{2} \mu_\nu)$$

Returning to the computation of the ratio of probabilities,

$$\begin{aligned} \frac{P(\epsilon_\delta | C_\ell)}{P(\epsilon_\delta^c | C_\ell)} &= \frac{P(C_\ell | \epsilon_\delta)}{P(C_\ell | \epsilon_\delta^c)} \frac{P(\epsilon_\delta)}{1 - P(\epsilon_\delta)} \\ &\geq \frac{1}{2} \frac{P(C_\ell | \epsilon_\delta)}{P(C_\ell | \epsilon_\delta^c)} P(\epsilon_\delta) \\ &\geq \frac{1}{2} \frac{P(C_\ell | \epsilon_\delta)}{P(C_\ell | \epsilon_\delta^c)} c_3^\ell (\delta)^\ell \\ &\geq \frac{1}{2} \frac{\exp(-2 \binom{\ell}{2} \delta)}{P(C_\ell | \epsilon_\delta^c)} c_3^\ell (\delta)^\ell \\ &\geq \frac{1}{2} \exp\left(-2 \binom{\ell}{2} \delta + 2 \binom{\ell}{2} |\mu_\nu| + \ell \log(c_3) + \log(\delta) \ell\right) \end{aligned}$$

therefore we can let $\delta = \exp(-|\tilde{\mu}_\nu| 2(\ell - 1))$ for any $|\tilde{\mu}_\nu| < |\mu_\nu|$ and therefore the proof is complete. \square

A.10 Proof of Lemma 9

Proof. We note that for a given set of nodes with equal latent positions, conditional on the node of interest appearing in a clique $\frac{d_i}{d_j} - \exp(\nu_i - \nu_j) = \mathcal{O}_P(n^{-1/2})$. Then since $\min_i \nu_i = \mathcal{O}_P(\exp(-|\tilde{\mu}_\nu| \ell))$. All of the random effects are converging to 0 and hence $\min_i \nu_i = \mathcal{O}_P\left(\min\left\{\exp(-|\tilde{\mu}_\nu| \ell), \frac{1}{\sqrt{n}}\right\}\right)$. \square

B Additional Computational Details

B.1 Newton Method for $\hat{\kappa}$

Given a set of distances \hat{d} we can estimate the curvature using a newton method. Firstly, we compute the derivative of $g(\kappa, d)$ with respect to κ .

$$\begin{aligned} \frac{\partial}{\partial \kappa} g(\kappa, d) &= (1/(4\kappa^2)) \left(8 \cos(d_{xm} \sqrt{\kappa}) - 4 \cos(d_{xz} \sqrt{\kappa}) \sec(d_{yz} \frac{\sqrt{\kappa}}{2}) \right. \\ &\quad + 4d_{xm} \sqrt{\kappa} \sin(d_{xm} \sqrt{\kappa}) \\ &\quad - 2d_{xy} \sqrt{\kappa} \sec(d_{yz} \frac{\sqrt{\kappa}}{2}) \sin(d_{xy} \sqrt{\kappa}) \\ &\quad - 2d_{xz} \sqrt{\kappa} \sec(d_{yz} \frac{\sqrt{\kappa}}{2}) \sin(d_{xz} \sqrt{\kappa}) \\ &\quad + d_{yz} \sqrt{\kappa} \cos(d_{xz} \sqrt{\kappa}) \sec(d_{yz} \frac{\sqrt{\kappa}}{2}) \tan(d_{yz} \frac{\sqrt{\kappa}}{2}) \\ &\quad \left. + \cos(d_{xy} \sqrt{\kappa}) \sec((d_{yz} \sqrt{\kappa})/2) (-4 + d_{yz} \sqrt{\kappa} \tan(d_{yz} \frac{\sqrt{\kappa}}{2})) \right) \end{aligned}$$

This allows us to construct a newton method for estimating the root $\hat{\kappa}$

$$\hat{\kappa}_{(m+1)} = \hat{\kappa}_{(m)} - \frac{g(\hat{\kappa}_{(m)}, \hat{d})}{\frac{\partial}{\partial \kappa} g(\hat{\kappa}_{(m)}, \hat{d})}$$

B.2 Distance Estimation

We recall the problem of estimating a distance matrix from a set of cliques \mathcal{C} . Though this problem is convex, due to the $O(K^3)$ restrictions in the problem, it the problem is often slow to reach a solution in CVXR. Instead, we solve this problem using a successive second order approximation.

$$\begin{aligned}
f(D) &:= \sum_{X,Y \in \mathcal{C}, i \in X, j \in Y} \left(A_{ij} (\nu_i + \nu_j - d_{xy}) \right. \\
&\quad \left. + (1 - A_{ij}) \log(1 - \exp(\nu_i + \nu_j - d_{xy})) \right) \\
&\approx \sum_{X,Y \in \mathcal{C}, i \in X, j \in Y} \left(A_{ij} (\nu_i + \nu_j - D_{0,x,y}) \right. \\
&\quad \left. + (1 - A_{ij}) \log(1 - \exp(\nu_i + \nu_j - D_{0,x,y})) \right. \\
&\quad \left. + \left((A_{ij} - 1) \frac{\exp(\nu_i + \nu_j - D_{0,x,y})}{1 - \exp(\nu_i + \nu_j - D_{0,x,y})} - A_{ij} \right) (d_{xy} - D_{0,x,y}) \right. \\
&\quad \left. + (A_{ij} - 1) \frac{\exp(\nu_i + \nu_j - D_{0,x,y})}{(1 - \exp(\nu_i + \nu_j - D_{0,x,y}))^2} \frac{(d_{xy} - D_{0,x,y})^2}{2} \right) \\
&:= \tilde{g}(D, D_0)
\end{aligned}$$

Hence to compute the global solution \hat{D} , we can iteratively solve the following optimization problem

$$\begin{aligned}
\hat{D}_{t+1} &= \operatorname{argsup}_{D \in \mathbb{R}^{\kappa \times \kappa}} \tilde{g}(D, \hat{D}_t) \\
D_{ij} &\geq 0 \quad \text{for all } i, j \\
\operatorname{Diag}(D) &= 0 \\
\operatorname{tr}(E_s^\top D) &\geq 0 \forall s \in \mathcal{S}
\end{aligned}$$

This process can be further sped up by choosing a good initialization matrix. We can do this by using the unconstrained maximum likelihood estimate \hat{D}_U , which is very fast to compute but does not enforce triangle inequality restrictions. This can be computed analogously as in theorem 10. Though many of the distances \hat{D}_U may not satisfy the triangle inequality, we can trim the distances so that \hat{D}_U form a distance matrix, and use this as the starting point. The Floyd-Warshall Algorithm is a possible option for constructing a distance matrix from a noisy matrix which might not have a distance structure. A natural extension to this in our context is seen in Algorithm 3.

One can draw similarities here to the problem of sparse metric repair. Metric repair seeks to adjust the fewest entries in a noisy distance matrix so that it still preserves the properties of being a metric (positivity, triangle inequality). Gilbert and Jain [2017] illustrated this Floyd-Warshall algorithm to be a solution to a special type known as decrease only metric repair.

C Other link functions:

Another common link function is the and formulation of the model is via the following:

$$\begin{aligned}
\nu_i &\sim F_\nu, \quad \nu_i \leq 0 \\
Z_i &\sim F_Z, \quad Z_i \in \mathcal{M}^p \\
P(G_{ij} = 1) &= \operatorname{logit}(\nu_i + \nu_j + \varphi - d(Z_i, Z_j))
\end{aligned}$$

Algorithm 3 Adapted Floyd-Warshall Algorithm

Require: $D \in \mathbb{R}_{\geq 0}^{K \times K}$ **Ensure:** $D = D^\top$

```
1: Trim entries below 0:  $D[D < 0] \leftarrow 0$ 
2: for  $k \in \{1, 2, \dots, n\}$  do
3:   for  $j \in \{1, 2, \dots, n\}$  do
4:     for  $i \in \{1, 2, \dots, n\}$  do
5:       if  $D_{ij} > (D_{ik} + D_{kj})$  then
6:          $D_{ij} \leftarrow (D_{ik} + D_{kj})$ 
7:       end if
8:     end for
9:   end for
10: end for
```

We can consistently estimate the node level parameters up to a constant shift using conditional maximum likelihood as in the semiparametric Rasch model [Andersen, 1970]. The parameter φ controls the global sparsity. Similar to before, we note that ν_i terms are likely to be very large in a cliques then we can set the largest parameter in each group to be nearly zero.

Other link functions may be used but will likely all need specific methods to estimate ν_i parameters within each clique. However, we have shown how it can be developed in these two canonical cases.

D Riemannian Geometry Definitions

In this section, we review some definitions of the sectional and scalar curvature as well as the volume elements. A Riemannian manifold $\mathcal{M} = (M, g)$ is a smooth manifold M equipped with a Riemannian inner product g_q on the tangent space $T_q(\mathcal{M})$ at any point $q \in \mathcal{M}$, $g_q(u, v) : T_q(\mathcal{M}) \times T_q(\mathcal{M}) \mapsto \mathbb{R}$.

This inner product can be used to define the Riemann curvature tensor at a point $q \in \mathcal{M}$ $R_q(u, v)w$, which takes 3 vectors u, v, w and returns an element of the tangent space

$$R_q(u, v)w : T_q(\mathcal{M}) \times T_q(\mathcal{M}) \times T_q(\mathcal{M}) \mapsto T_q(\mathcal{M})$$
$$R_q(u, v)w := [\nabla_u, \nabla_v]w - \nabla_{[u, v]}w$$

where $[u, v]$ is the lie bracket of vector fields and $[\nabla_u, \nabla_v]$ is the commutator of differential operators. The Riemann curvature tensor can be used to define our main quantity of interest, the sectional curvature at a point $\kappa_q(u, v) : \times T_q(\mathcal{M}) \times T_q(\mathcal{M}) \mapsto \mathbb{R}$. The sectional curvature takes two linearly independent elements of the tangent space and maps them to the real line.

$$\kappa_q(u, v) := \frac{g_q(R_q(u, v)v, u)}{g_q(u, u)g_q(v, v) - g_q(u, v)^2}$$

The sectional curvature is independent of the coordinate system used, but depends only on the linear subspace spanned by u, v . Furthermore, in the canonical

manifolds $\kappa_q(u, v) = \kappa$ by construction.

From the sectional curvature, we can define the scalar curvature $S(m)$,

$$S(q) := \sum_{i \neq j} \kappa(e_i, e_j)$$

where $\{e_i\}_{i=1}^p$ form an orthonormal frame for $T_q(\mathcal{M})$. We can think of the scalar curvature as an “average of sectional curvatures” across the manifold.

We next define a volume form (also known as the Levi-Civita Tensor) via the Riemannian inner product g . If ω is a local oriented coordinate system near a point q then

$$dV := \sqrt{|\det(g)|} d\omega.$$

where g_q is the metric tensor evaluated on the basis coordinate system ω . For further details on these quantities, see Klingenberg [1995].

From this definition of a volume, we can define probability density functions on the manifold. A density function f corresponding to a measure F with support on the manifold can be defined as follows. For a set $\mathcal{X} \subset \mathcal{M}$.

$$P(X \in \mathcal{X}) = \int_{x \in \mathcal{X}} f(x) dV_x$$

See Pennec [1999] for further introduction for defining probabilities on the manifold.

E Assumptions on \mathcal{M}

Here we verify that the Algebraic Midpoint properties, as well as locally Euclidean properties are satisfied for a complete simply connected smooth Riemannian manifolds.

If the algebraic midpoint property is satisfied for any complete metric space \mathfrak{M} then by Theorem 1.8 of Gromov [2007], then \mathfrak{M} is a **path metric space**. The authors follow up in discussion a list of examples of path metric spaces, which include Riemannian manifolds with boundary.

Secondly, if \mathcal{M}^p has scalar curvature at point q , $S(q)$ then

$$\frac{\text{Vol}(B_{\mathcal{M}^p}(\epsilon, q))}{\text{Vol}(B_{\mathbb{E}^p}(\epsilon, q))} = 1 - \frac{S(q)}{6(p+2)} \epsilon^2 + o(\epsilon^3)$$

by Theorem 3.98 of Gallot et al. [2004]. Since this holds, then for a latent metric which is generated by distances on a Riemannian manifold, the locally Euclidean volume property will hold.

F Graph Statistics From Simulations

Columns denote the scale factor used in the simulations.

Table 4: $\kappa = -2$ graph statistics summary.

Scale (ρ)	0.7	1	2
Edge.fraction	0.016 (0.001)	0.012 (0.001)	0.007 (0.001)
Max.Degree	341.3 (23.596)	412.29 (26.364)	656.63 (33.954)
Mean.Degree	56.726 (5.279)	58.538 (5.351)	73.975 (5.448)
Distinct.Cliques $\geq \ell$	78.665 (6.955)	53.675 (5.427)	43.515 (4.41)
Max.Clique.Size	24.215 (4.985)	28.725 (5.494)	NaN (NA)
Mean.Degree.Centrality	0.155 (0.009)	0.134 (0.007)	0.107 (0.005)

Table 5: $\kappa = -1$ graph statistics summary.

Scale (ρ)	0.7	1	2
Edge.fraction	0.017 (0.002)	0.012 (0.001)	0.008 (0.001)
Max.Degree	343.69 (25.21)	416.825 (28.796)	661.12 (32.257)
Mean.Degree	58.943 (5.354)	61.168 (5.636)	78.239 (5.6)
Distinct.Cliques $\geq \ell$	80.14 (6.488)	54.965 (5.404)	42.32 (5.027)
Max.Clique.Size	24.005 (5.456)	28.735 (6)	NaN (NA)
Mean.Degree.Centrality	0.159 (0.008)	0.137 (0.007)	0.112 (0.005)

Table 6: $\kappa = -0.5$ graph statistics summary.

Scale (ρ)	0.7	1	2
Edge.fraction	0.017 (0.001)	0.013 (0.001)	0.008 (0.001)
Max.Degree	340.785 (21.648)	413.115 (24.818)	656.07 (39.433)
Mean.Degree	59.658 (4.776)	62.67 (4.989)	79.873 (6.566)
Distinct.Cliques $\geq \ell$	80.205 (6.493)	55.155 (5.288)	39.95 (5.289)
Max.Clique.Size	23.62 (5.216)	29.52 (6.073)	NaN (NA)
Mean.Degree.Centrality	0.161 (0.009)	0.141 (0.007)	0.114 (0.005)

Table 7: $\kappa = 0$ graph statistics summary.

Scale (ρ)	0.7	1	2
Edge.fraction	0.012 (0.001)	0.008 (0)	0.005 (0)
Max.Degree	205.38 (16.619)	242.88 (18.178)	371.805 (24.336)
Mean.Degree	40.815 (2.626)	41.759 (2.415)	52.465 (2.813)
Distinct.Cliques $\geq \ell$	70.2 (13.19)	46.84 (6.057)	41.54 (4.576)
Max.Clique.Size	23.735 (5.244)	28.49 (5.421)	41.63 (7.913)
Mean.Degree.Centrality	0.169 (0.017)	0.149 (0.013)	0.125 (0.009)

Table 8: $\kappa = 0.5$ graph statistics summary.

Scale (ρ)	0.7	1	2
Edge.fraction	0.017 (0.001)	0.013 (0.001)	0.008 (0)
Max.Degree	267.08 (17.432)	318.615 (18.062)	488.545 (25.046)
Mean.Degree	61.311 (2.803)	63.539 (2.96)	80.373 (3.454)
Distinct.Cliques $\geq \ell$	87.945 (12.778)	55.385 (7.343)	39.535 (5.591)
Max.Clique.Size	23.595 (4.844)	28.45 (6.158)	39.925 (7.861)
Mean.Degree.Centrality	0.21 (0.016)	0.183 (0.012)	0.153 (0.008)

Table 9: $\kappa = 1$ graph statistics summary.

Scale (ρ)	0.7	1	2
Edge.fraction	0.025 (0.001)	0.018 (0.001)	0.012 (0)
Max.Degree	351.89 (16.965)	421.36 (18.32)	652.265 (26.131)
Mean.Degree	88.331 (3.89)	91.901 (3.805)	117.569 (4.089)
Distinct.Cliques $\geq \ell$	91.71 (30.245)	64.23 (17.006)	41.765 (4.761)
Max.Clique.Size	24.07 (5.334)	29.29 (6.259)	40.52 (7.969)
Mean.Degree.Centrality	0.241 (0.012)	0.21 (0.01)	0.174 (0.007)